NASA TECHNICAL NOTE

NASA TN D-4122

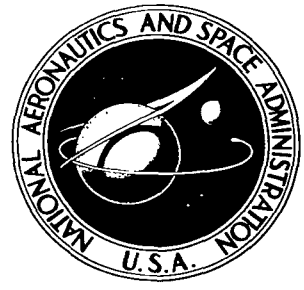

NASA TN D-4122

AERODYNAMIC CHARACTERISTICS OF THREE AXISYMMETRIC LOW-FINENESS-RATIO REENTRY SHAPES AT MACH 6.9

by Jim A. Penland and Peter T. Bernot

Langley Research Center
Langley Station, Hampton, Va.

NATIONAL AERONAUTICS AND SPACE ADMINISTRATION • WASHINGTON, D. C. • AUGUST 1967

AERODYNAMIC CHARACTERISTICS OF THREE AXISYMMETRIC LOW-FINENESS-RATIO REENTRY SHAPES AT MACH 6.9

By Jim A. Penland and Peter T. Bernot

Langley Research Center
Langley Station, Hampton, Va.

NATIONAL AERONAUTICS AND SPACE ADMINISTRATION

For sale by the Clearinghouse for Federal Scientific and Technical Information
Springfield, Virginia 22151 – CFSTI price $3.00

AERODYNAMIC CHARACTERISTICS OF THREE AXISYMMETRIC LOW-FINENESS-RATIO REENTRY SHAPES AT MACH 6.9

By Jim A. Penland and Peter T. Bernot
Langley Research Center

SUMMARY

An experimental investigation has been conducted to determine the force, stability, and control characteristics of three low-fineness-ratio axisymmetric reentry shapes at a Mach number of 6.9 and a Reynolds number based on body length of 0.98×10^6. Analysis of the data indicates that trim may be accomplished by the use of trailing-edge flap controls and that a wide trim angle-of-attack range may be provided by a downward shift of the center of gravity. With moderate afterbody alteration and appropriate center-of-gravity location, an axisymmetric body may be made self-trimming. Newtonian theory for the basic bodies without controls provided good estimates of normal force, pitching moment, and center-of-pressure location but optimistic estimates of maximum lift-drag ratio.

INTRODUCTION

A number of studies have shown that the use of lift during reentry makes possible a relaxation of guidance requirements due to the enlargement of the entry corridor, and increase in maneuverability, the alleviation of aerodynamic heating rates, and a decrease in deceleration. In addition, certain of these studies (e.g., refs. 1 and 2) have indicated that reentry vehicles having hypersonic maximum lift-drag ratios in the vicinity of unity merit further investigation. One class of vehicles which could provide this medium lift-drag ratio are the axisymmetric configurations described in this report. The experimental hypersonic aerodynamic characteristics have been determined for three shapes, with particular emphasis placed on the longitudinal stability and control characteristics and on the evaluation of performance losses associated with attaining static stability over the range of lift-drag ratios from 0 to the maximum value. The effects of center-of-gravity location, of control-flap deflection, and of afterbody geometry on stability and trim were explored in this range. Two double conical bodies and a minimum-drag configuration were tested at a Mach number of 6.9 in the Langley 11-inch hypersonic tunnel; the test

Reynolds numbers approached 10^6. The data are compared with Newtonian calculations; viscous effects are also included in the calculations.

SYMBOLS

A_b	model-base area
C_A	axial-force coefficient, $(F_A - F_b)/q_\infty A_b$
C_D	drag coefficient, $F_D'/q_\infty A_b$
C_F	average skin-friction coefficient
C_L	lift coefficient, $F_L/q_\infty A_b$
$(C_L)_t$	C_L at trim condition
C_l	rolling-moment coefficient, $M_X/q_\infty A_b l$
C_{l_β}	rate of change of rolling-moment coefficient with angle of sideslip
C_m	pitching-moment coefficient, $M_Y/q_\infty A_b l$
C_{m_α}	rate of change of pitching-moment coefficient with angle of attack, $\partial C_m/\partial\alpha$
$(C_{m_\alpha})_t$	C_{m_α} at trim condition
C_N	normal-force coefficient, $F_N/q_\infty A_b$
C_n	yawing-moment coefficient, $M_Z/q_\infty A_b l$
C_{n_β}	rate of change of yawing-moment coefficient with angle of sideslip
$C_{p,max}$	maximum or stagnation pressure coefficient
C_Y	side-force coefficient, $F_Y/q_\infty A_b$
C_{Y_β}	rate of change of side-force coefficient with angle of sideslip

d	base diameter of model 1, 2.50 inches (6.35 centimeters)
F_A	axial force along X-axis (positive direction is -X)
F_b	base-pressure correction, $(p_\infty - p_b)A_b$
$F_D' = F_N \sin \alpha + (F_A - F_b)\cos \alpha$	
$F_L = F_N \cos \alpha + (F_b - F_A)\sin \alpha$	
F_N	normal force along Z-axis (positive direction is -Z)
F_Y	side force along Y-axis
L/D	lift-drag ratio, C_L/C_D
$(L/D)_{max}$	maximum L/D
$(L/D)_t$	trim L/D
l	model length
M	free-stream Mach number
M_X, M_Y, M_Z	rolling, pitching, and yawing moments, respectively
n	length of afterbody slice, measured along stagnation line from model base
p_b	base pressure
p_∞	free-stream static pressure
q_∞	free-stream dynamic pressure
R	free-stream Reynolds number based on l unless otherwise stated
X,Y,Z	reference axes
x	longitudinal distance, measured along X-axis from model nose

x_{cg}	longitudinal distance of center of gravity from model nose
x_{cp}	longitudinal distance of center of pressure from model nose
y	radial distance, measured along Y-axis from model center line
z_{cg}	vertical distance of center of gravity from model center line
α	angle of attack
α_t	trim angle of attack
β	angle of sideslip
δ_B	angle of bottom-control deflection
δ_T	angle of top-control deflection

APPARATUS AND TEST CONDITIONS

The tests were conducted in the Mach 6.86 test section of the Langley 11-inch hypersonic tunnel. The tunnel-wall boundary-layer thickness and hence the free-stream Mach number are dependent upon the stagnation pressure. For these tests, the stagnation pressure was 13 atmospheres (1.32×10^6 newtons/meter^2) for model 2 and was 18 atmospheres (1.82×10^6 newtons/meter^2) for models 1, 1a, and 3. The average stagnation temperature was about 640° F (611° K) for all tests (to avoid liquefaction). The stagnation pressures of 13 atmospheres (1.32×10^6 N/m^2) and 18 atmospheres (1.82×10^6 N/m^2) resulted in average free-stream Mach numbers of 6.81 and 6.85, respectively, and average Reynolds numbers per inch (per 2.54 centimeters) of 0.142×10^6 and 0.192×10^6, respectively. The absolute humidity was kept to less than 1.9×10^{-5} parts of water per part of dry air by weight for all tests.

All force and moment measurements were made by using a six-component water-cooled strain-gage internal balance. Readout was continuously recorded on pen-marked strip-chart self-balancing potentiometers.

Tests were conducted through an angle-of-attack range of 0° to 25° for model 2 and -16° to 16° for models 1, 1a, and 3. Base pressures were measured and the axial-force component was adjusted to correspond to a base pressure equal to the free-stream static pressure.

MODELS

A photograph of the models used in this investigation is presented in figure 1, and dimensions based on the diameter of model 1, which was 2.50 inches (6.35 centimeters) are given in figure 2. All models were constructed of stainless steel, and the control surfaces of model 1 were made from 21-gage sheet brass attached to trailing edge of the body with flat-head screws and faired to body contour upstream of the hinge line. The control-surface area was equal to 5.1 percent of the model-base area. Model 1a was similar to model 1 except for the slices removed from the afterbody. Model 2 was an elongated version of model 1. Model 3 was a minimum-drag shape having the same length and volume as model 1 but whose external contour (sharp-nose version only) conforms to that determined as optimum for a given length and volume (see ref. 3).

PRECISION OF DATA

The maximum uncertainties in the measurement of the force and moment coefficients for the individual test points as a result of inaccuracies in the force balance readout system are presented as follows, with model 1 used as the reference:

C_N . . . . . ±0.0044
C_A . . . . . ±0.0014
C_m . . . . . ±0.001

The stagnation pressure was measured to an accuracy of ±1.5 inches of mercury (5079.58 N/m^2) and the Mach number was known to ±0.01. The corresponding accuracy of free-stream dynamic pressure was ±0.02 lb/in^2 (137.9 N/m^2). The angles of attack were set to an accuracy of ±0.20° and the control deflections, to an accuracy of ±0.20°.

RESULTS AND DISCUSSION

The results of all tests and calculations are presented in coefficient form, with the longitudinal data referred to the stability-axis system and the directional and lateral data to the body-axis system (see fig. 3). The moment reference is on the model geometric center line at a body station 62 percent of the model length from the nose unless otherwise specified.

Longitudinal Aerodynamic Characteristics

Basic data.- The basic longitudinal control data for model 1 with various deflections of a single flap located on the bottom of the double conical body are presented in figure 4 through an angle-of-attack range of -16° to 16°. It should be noted that the data shown

at negative angles of attack for the various control deflections of the bottom flap may be also considered as data taken at positive angles of attack with a top control. The use of top controls is discussed subsequently. Figure 4(a) shows that deflection of the single bottom flap produces a substantial pitching-moment increase at positive angles of attack and a rather abrupt loss in control effectiveness as the flap enters the shadowed region created by the body at negative angles of attack. The normal-force, axial-force, lift, and drag coefficients (see figs. 4(a) and 4(b)) increase with bottom-control deflection at positive angles of attack but the lift-drag ratio decreases.

The basic longitudinal data for model 1 with two trailing-edge bottom controls (each having an area equal to 5.1 percent of the model base area) are presented in figure 5. The effectiveness of the two identical closely spaced flaps as compared with that of the single flap (fig. 4) is determined. The variations of all longitudinal parameters with angle of attack and control deflection are similar to those for the single flap. A comparison of the single-control and the two-control tests showed that the effectiveness of the two controls was approximately double that of the single control.

In order to determine if the basic model 1 could be made self-trimming at positive angles of attack with the center of gravity on the geometric center line, tests were made after the removal of various afterbody slices (removal of wedge-shaped slabs from the trailing edge). (See fig. 2.) The results for model 1a, presented in figure 6, show a marked change in all longitudinal characteristics because of these configuration modifications. Both the normal-force and the axial-force coefficients decreased at positive angles of attack and the pitching-moment curves exhibited a pronounced destabilizing trend with increasing afterbody slice (fig. 6(a)). Figure 6(b) shows that the lift coefficient, drag coefficient, and lift-drag ratio also decreased with afterbody alteration. At negative angles of attack the region that includes the afterbody slice is within the wake or is shadowed and therefore is only slightly affected by variations in afterbody slice. The results of tests on an elongated version of model 1, which was designated model 2, are presented in figure 7. This configuration was found to have improved lift-drag characteristics but less desirable pitching-moment characteristics than model 1 or model 1a, as evidenced by the unstable slope of the curve for C_m as a function of α in figure 7(a).

In an attempt to improve the maximum lift-drag ratio, a configuration having the same overall length and volume as model 1 but having a shape contoured for minimum drag was investigated. This configuration, designated model 3, was designed by using the concept presented in reference 3. The contour selected was optimized on the basis of length and volume, and the model was tested first with a sharp nose and later with a blunt nose like that of model 1. The results of these tests are presented in figure 8 and show only slight losses in lift-drag ratio due to nose bluntness. Compared with model 1 having no flap deflection (fig. 4(b)), the blunted model 3 showed about 7 percent improvement in

maximum lift-drag ratio but was unstable in pitch at the chosen center-of-gravity location $\left(x_{cg}/l = 0.62\right)$.

Schlieren photographs of various configurations are presented in figures 9 to 12. Model 1 with and without flap deflection is shown in figure 9. Enlarged views of the intricate flow and shock pattern in the vicinity of the flaps are shown in figure 10, and the angles of attack of 0° and 12° correspond to the approximate angles for zero lift and maximum lift-drag ratio, respectively. Note in figure 10 what appears to be separation-induced shocks ahead of the flap as well as the shock due to the flap-deflected flow.

Comparison of theory and experiment.- Theoretical analysis of bodies of revolution through an angle-of-attack range can readily be handled with Newtonian impact theory, particularly when the bow shock wave is detached. Such an analysis was made on models 1, 2, and 3 by using a value of $C_{p,max}$ of 2.00, and the longitudinal results are presented in figures 13 and 14. The average laminar skin-friction coefficient C_F, which was assumed to be equal to that of a conical body having the same length and volume as the model under analysis, was estimated by the method of reference 4 and added to the axial-force components at all angles of attack.

The prediction of normal-force and pitching-moment coefficients – not only the magnitude but also the slope of the curves with angle of attack – is seen to be excellent (fig. 13). Thus, good predictions of center-of-pressure location were obtained (fig. 14). The predictions of axial-force coefficients (fig. 13) were improved with the addition of C_F, but the axial force was in general underpredicted at all angles of attack. This underpredicted axial force, when combined with more reasonable normal force, resulted in an underpredicted drag coefficient and an optimistic maximum lift-drag ratio. The relatively small variation of the longitudinal characteristics due to nose bluntness may be seen in figure 13(c) for model 3.

An attempt was made to calculate the flap effectiveness for model 1 by Newtonian, tangent-cone, and tangent-wedge theories, with the schlieren photographs in figure 10 used as an aid in estimating local dynamic pressures. These methods were found to be inadequate and from these studies it was concluded that present theoretical methods are not adequate for predicting local pressures in regions behind multiple shocks and/or regions of three-dimensional flow.

Effects of center-of-pressure location.- A comparison of the center-of-pressure location at various angles of attack and the center-of-gravity location is presented in figure 14 for models 1, 2, and 3. The center-of-gravity locations in figure 14 were those calculated for solid homogeneous bodies and therefore are not necessarily representative of full-scale operational vehicles. The center of pressure is shown to vary only slightly with angle of attack for any of the three configurations, but its location is significantly different for each shape. Of importance is the proximity of the geometric center of gravity

to the aerodynamic center of pressure. The center of pressure, as shown in figure 14, is ahead of the center of gravity of the solid models 1, 2, and 3 by 8.2, 15.49, and 13.45 percent body length, respectively. Inasmuch as the center of gravity of model 1 needs to be moved forward only 8.2 percent body length, it may be concluded that, from the practical standpoint of obtaining a statically stable configuration, model 1 is the best of the three shapes considered, notwithstanding the higher maximum lift-drag ratio of the minimum-drag shape. Model 1 was therefore selected for further analysis.

Effects of center-of-gravity location.- From figure 14 it may be seen that the center of pressure on model 1 does not vary more than about 1 percent body length through the 16° angle-of-attack range. The maximum lift-drag ratio occurred at an angle of attack of about 12.9° (fig. 4) for the basic model 1 without flaps. Thus with an off-axis center-of-gravity location the vehicle could be made self-trimming at a positive angle of attack. The results of such a study for variations of longitudinal as well as vertical center-of-gravity location for trim are presented in figure 15. Both the distance x_{cg}, measured from the model nose, and the distance z_{cg}, measured from the geometric center line, are presented as percentages of the body length. It may be seen that with the proper selection of center-of-gravity location the basic vehicle may be made self-trimming through the angle-of-attack range up to and including the angle for maximum lift-drag ratio. It is unlikely that the wide trim capability shown in figure 15 can be realized because of the practical problems of packaging equipment within a given vehicle; however, center-of-gravity locations as far forward as $x_{cg}/l = 0.62$ and as far beneath the center line as $z_{cg}/l = 0.03$ do not seem unreasonable. Some in-flight variation of center-of-gravity location may also be possible. The use of fixed off-center center-of-gravity locations in conjunction with aerodynamic controls for increasing the trim range appears entirely feasible.

Effects of control deflection.- Figure 16 presents the results of a study in which the bottom and top controls on model 1 were deflected for various vertical center-of-gravity locations while the longitudinal center-of-gravity location was held constant at $x_{cg}/l = 0.62$. This study indicates that movement of the center of gravity is a much more effective way of trimming to positive angles of attack near maximum lift-drag ratio than the use of aerodynamic controls. However, a combination of a downward or positive vertical shift of the center of gravity and aerodynamic-control deflection makes possible the trimming of the vehicle from zero to maximum L/D. This trim range covers a wide range of lift conditions and exhibits positive static longitudinal stability at all angles of attack.

The curves of pitching moment as a function of angle of attack for model 1a, after removal of various afterbody slices, are presented in figure 6 for a center-of-gravity location of $x_{cg}/l = 0.62$. These data for the angle-of-attack range of 0° to 16° are

presented in figure 17 along with the same data transferred to that longitudinal body station necessary for trim near $(L/D)_{max}$. This figure shows that, with the proper center-of-gravity location, model 1a may be made self-trimming at the respective angle of attack for $(L/D)_{max}$ for each size of afterbody slice. These configurations exhibit a small margin of positive longitudinal stability at trim.

Lateral-Directional Characteristics

It is well known that, by the rotation of axes, data at combined angles of attack and sideslip may be obtained from longitudinal data for axisymmetric bodies of revolution. Data for model 1 without controls, as presented in figure 4, were thus reoriented to provide the lateral-directional characteristics presented in figure 18. These data indicate that model 1 has favorable static directional stability at angles of attack up to 16° and that the level of positive effective dihedral may be varied by the vertical movement of the center of gravity.

CONCLUSIONS

Analysis of experimental data obtained on a series of axisymmetric reentry configurations at a Mach number of 6.9 and a Reynolds number based on model length of 0.98×10^6 leads to the following conclusions:

1. Trim may be accomplished by the use of trailing-edge flap controls, but a loss of effectiveness is realized when the control is within a shadowed region.

2. A combination of aerodynamic-control deflection and a downward shift of the center of gravity provides a wide trim angle-of-attack range for an axisymmetric reentry body.

3. The alteration of the afterbody by removal of volume from the lower trailing edge in combination with the appropriate longitudinal center-of-gravity location can provide an inherent self-trimming capability at maximum lift-drag ratio for an axisymmetric reentry body.

4. For a fixed longitudinal center-of-gravity location, the elongation of a body, while improving the lift-drag characteristics, can produce less desirable pitch characteristics.

5. For a given vehicle length and volume, a theoretically designed minimum-drag body provided a greater maximum lift-drag ratio than its cone-frustum counterpart, but this improvement was accompanied by an undesirable forward movement of the center of pressure.

6. The use of Newtonian theory on the bodies of revolution without controls provided excellent predictions of normal-force and pitching-moment coefficients and

center-of-pressure location but underestimated axial-force coefficients and thus optimistic values of maximum lift-drag ratio.

Langley Research Center,
National Aeronautics and Space Administration,
Langley Station, Hampton, Va., January 20, 1967,
124-07-02-57-23.

REFERENCES

1. Love, Eugene S.: Factors Influencing Configuration and Performance of Multipurpose Manned Entry Vehicles. J. Spacecraft Rockets, vol. 1, no. 1, Jan.-Feb. 1964, pp. 3-12.

2. Love, Eugene S.: Manned Lifting Entry. Astronaut. Aeron., vol. 4, no. 5, May 1966, pp. 54-64.

3. Miele, Angelo: Optimum Slender Bodies of Revolution in Newtonian Flow. Tech. Rept. No. 56, Flight Sci. Lab., Boeing Sci. Res. Lab., Apr. 1962.

4. Penland, Jim A.: A Study of the Stability and Location of the Center of Pressure on Sharp, Right Circular Cones at Hypersonic Speeds. NASA TN D-2283, 1964.

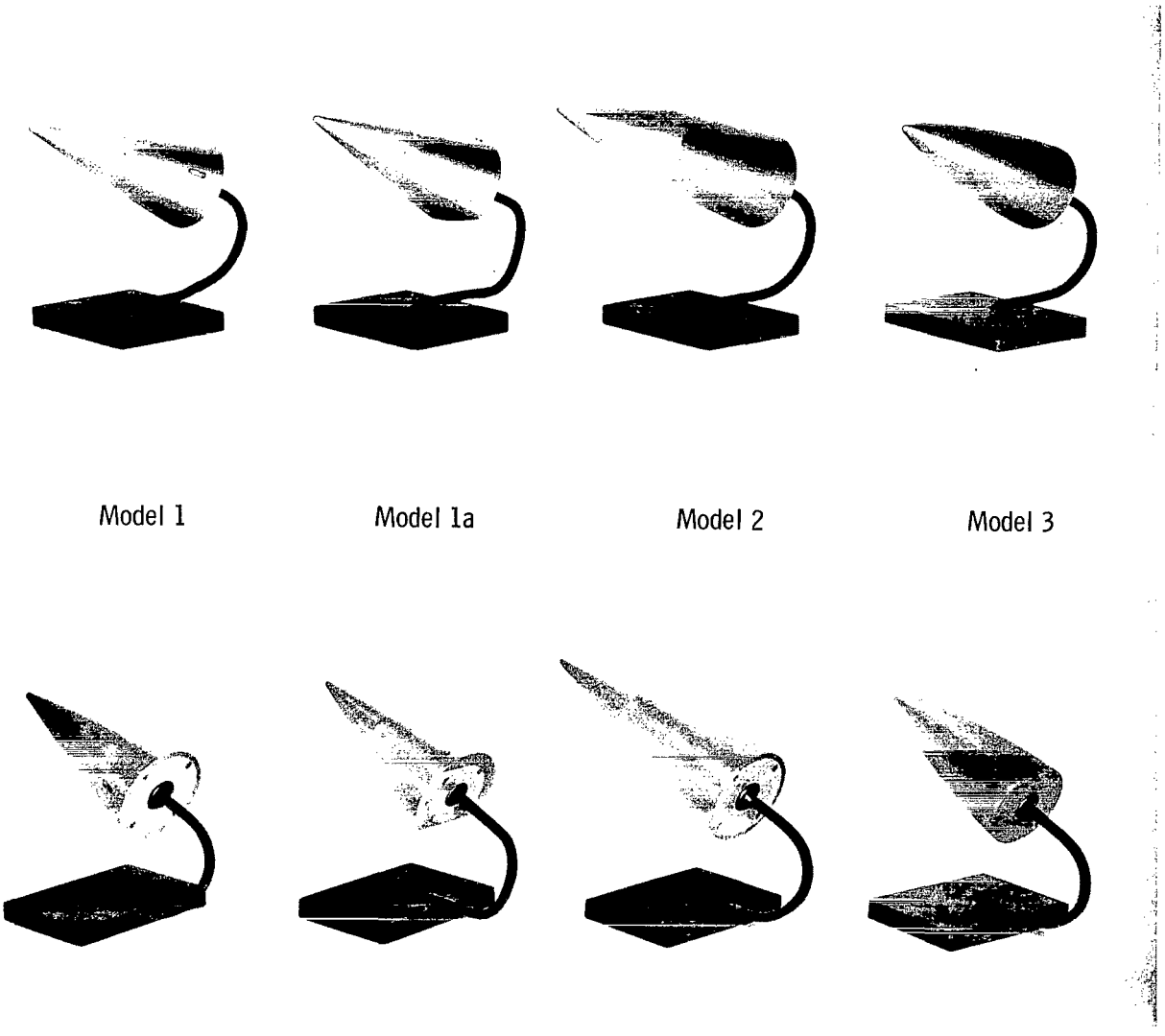

Figure 1.- Photograph of models.

L-67-959

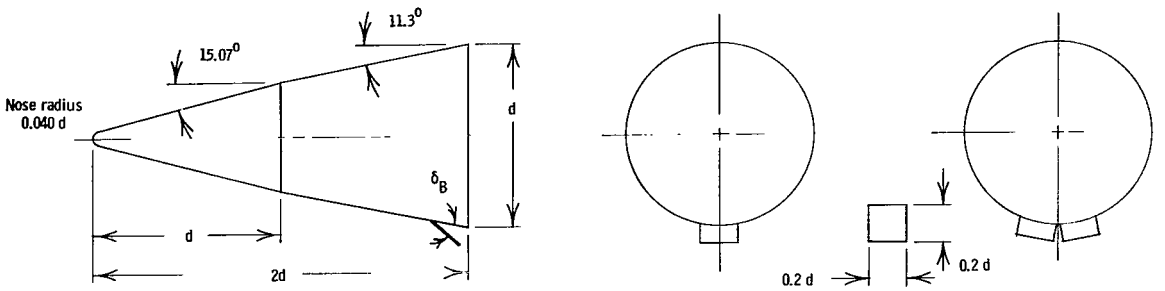

Model 1

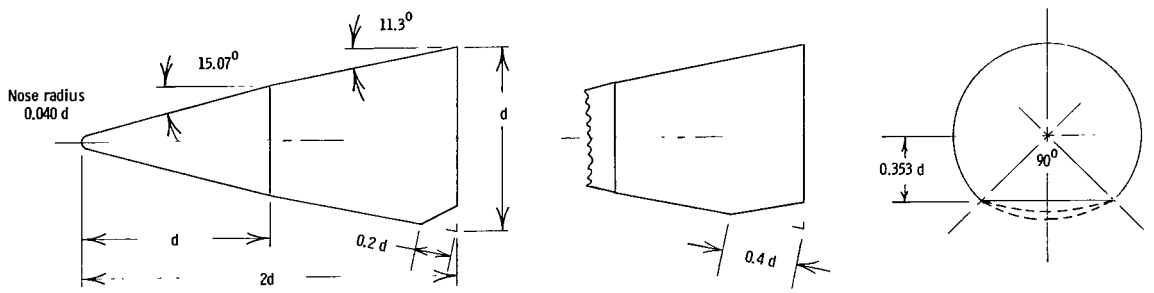

Model 1a

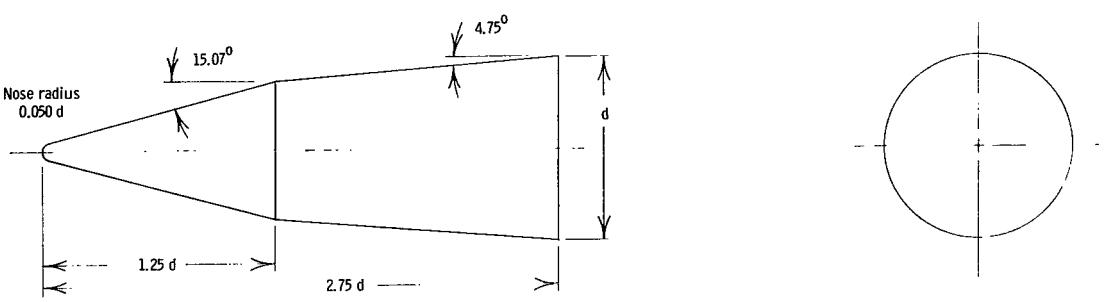

Model 2

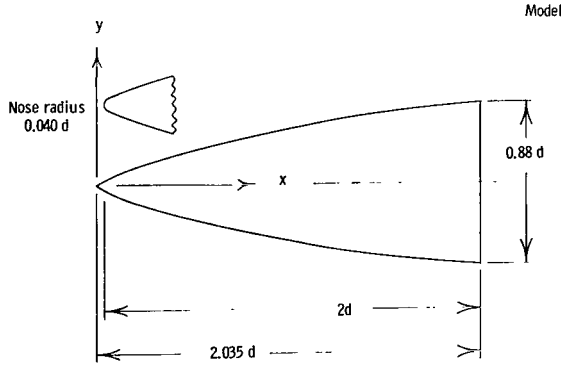

x/d	y/d
0	0
.0408	.0292
.1020	.0592
.1748	.0880
.3028	.1320
.4480	.1760
.7820	.2640
1.0076	.3080
1.2216	.3472
1.4252	.3796
1.6288	.4092
1.7588	.4224
2.0360	.4400

Model 3

Figure 2.- Details of models, with dimensions based on diameter of model 1 (d = 2.50 in. (6.35 cm)).

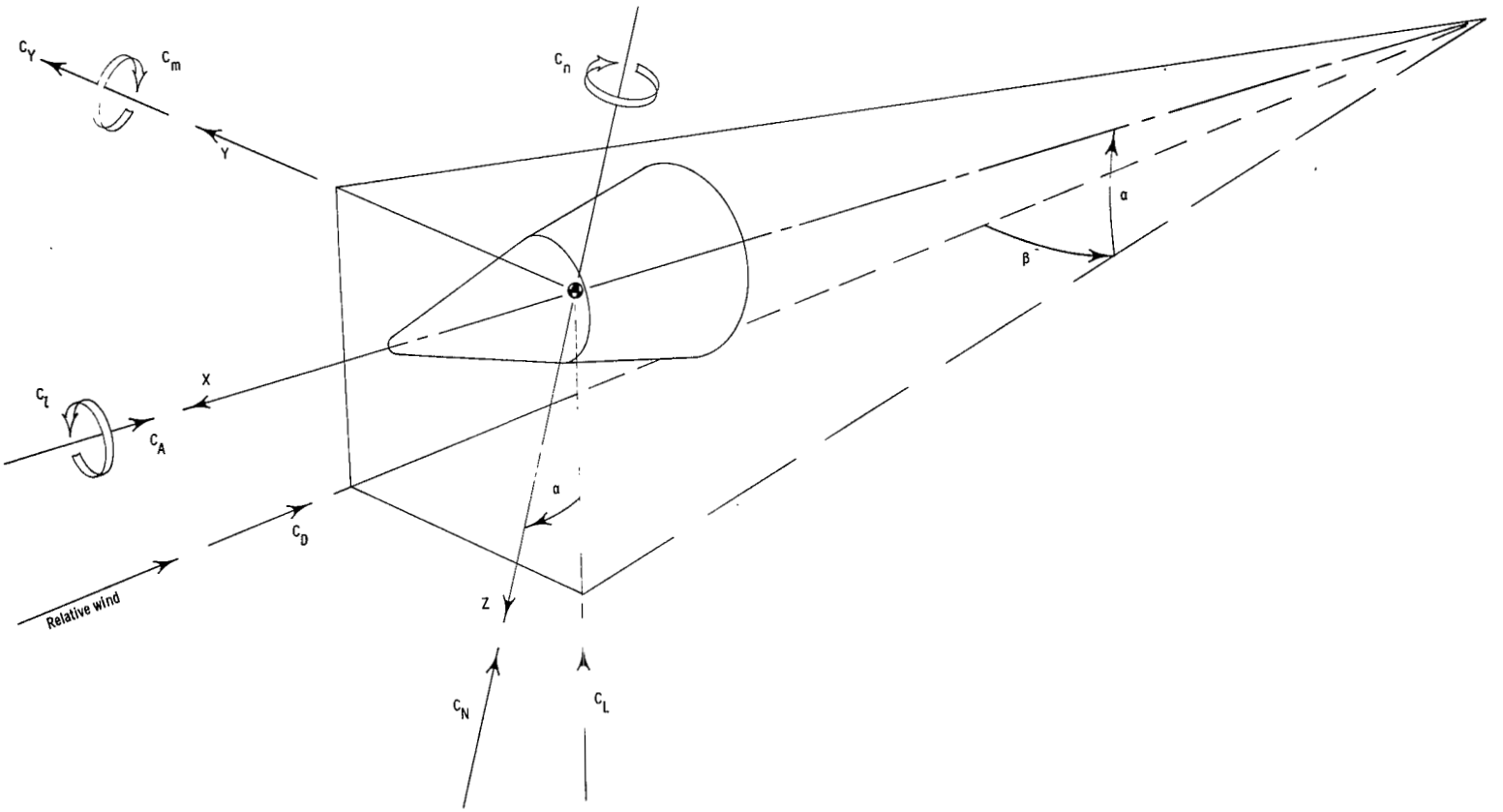

Figure 3.- Axis system. (Arrows indicate positive direction.)

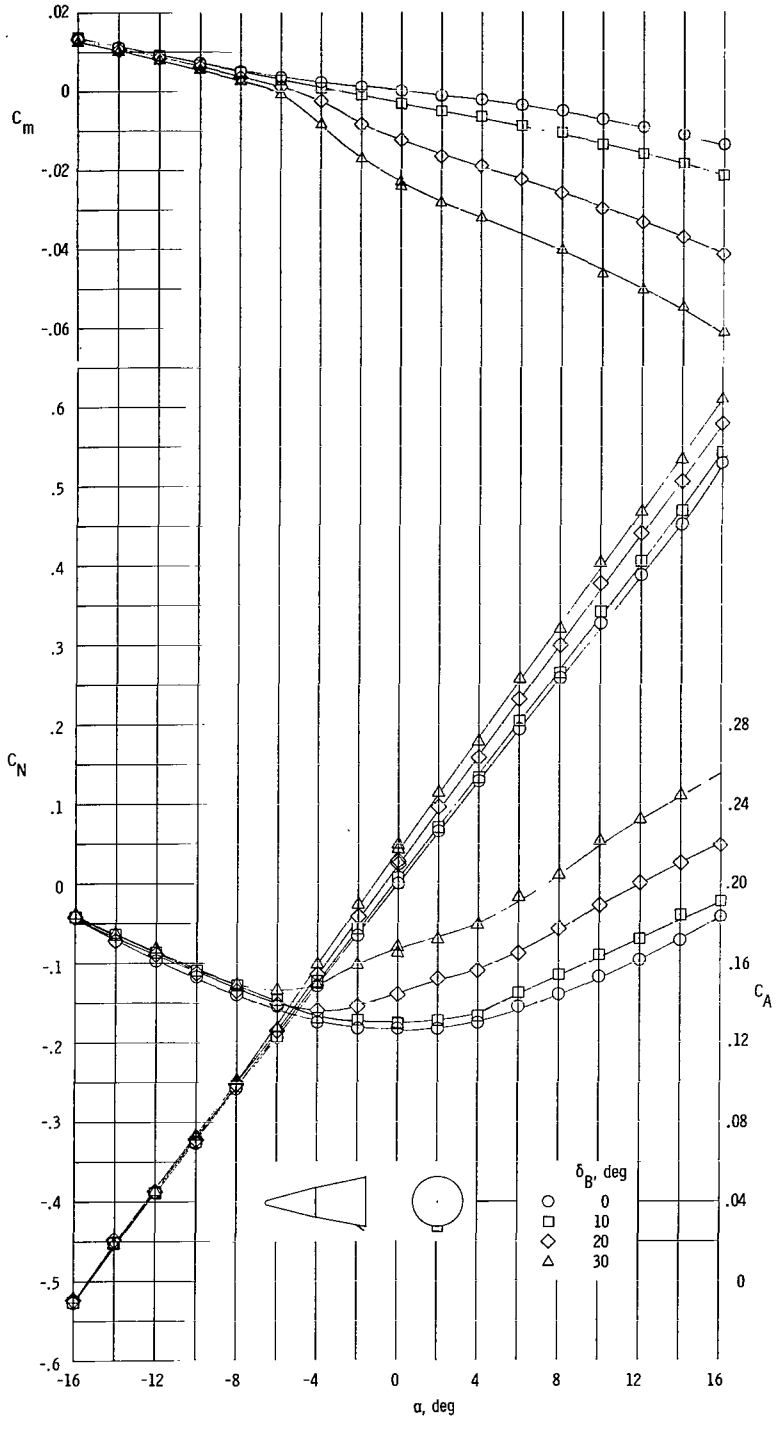

(a) Pitching-moment, normal-force, and axial-force coefficients.

Figure 4.- Basic longitudinal data for model 1 with various single-bottom-flap deflections. M = 6.9; R = 0.98 × 10^6.

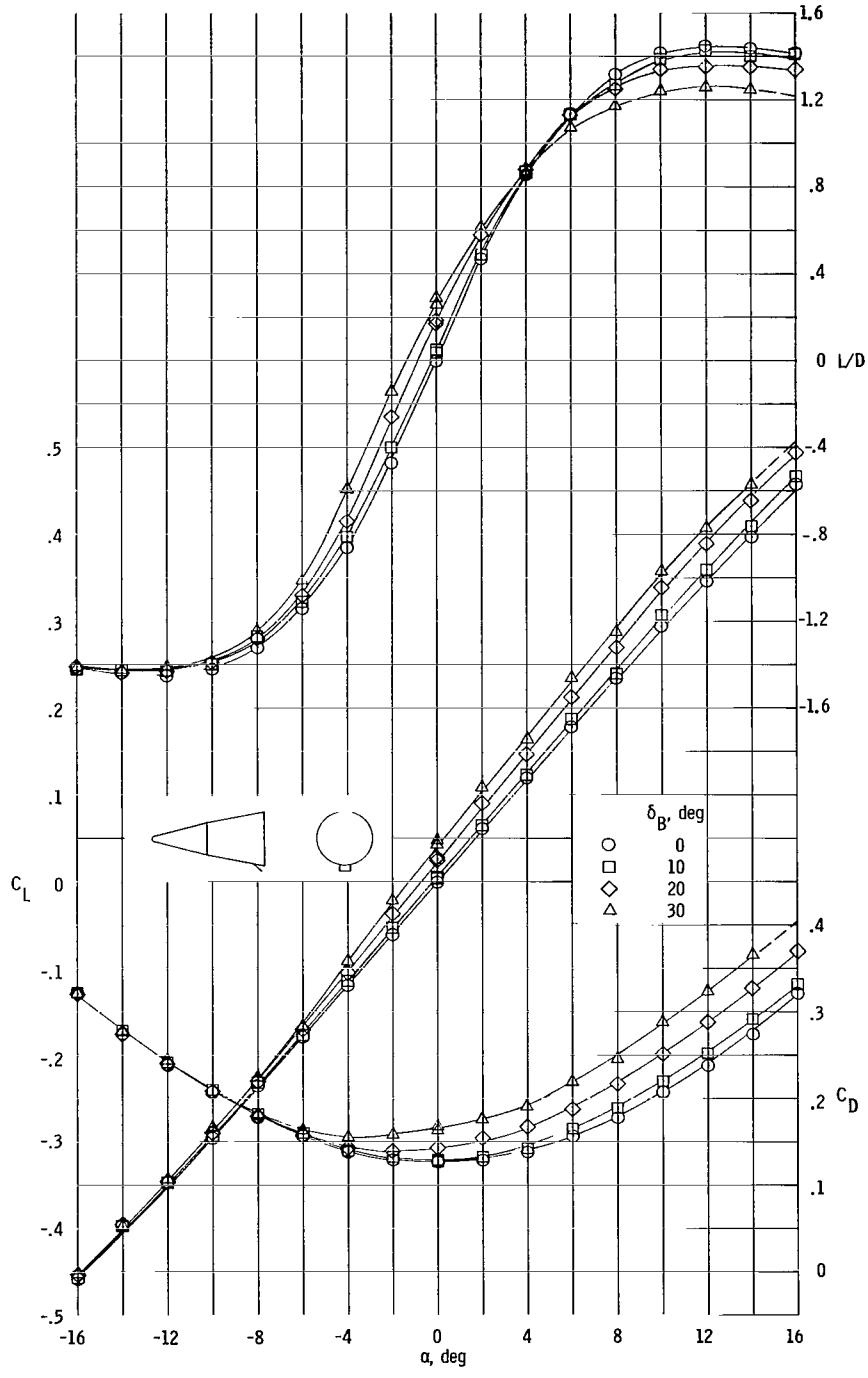

(b) Lift-drag ratio, lift coefficient, and drag coefficient.

Figure 4.- Concluded.

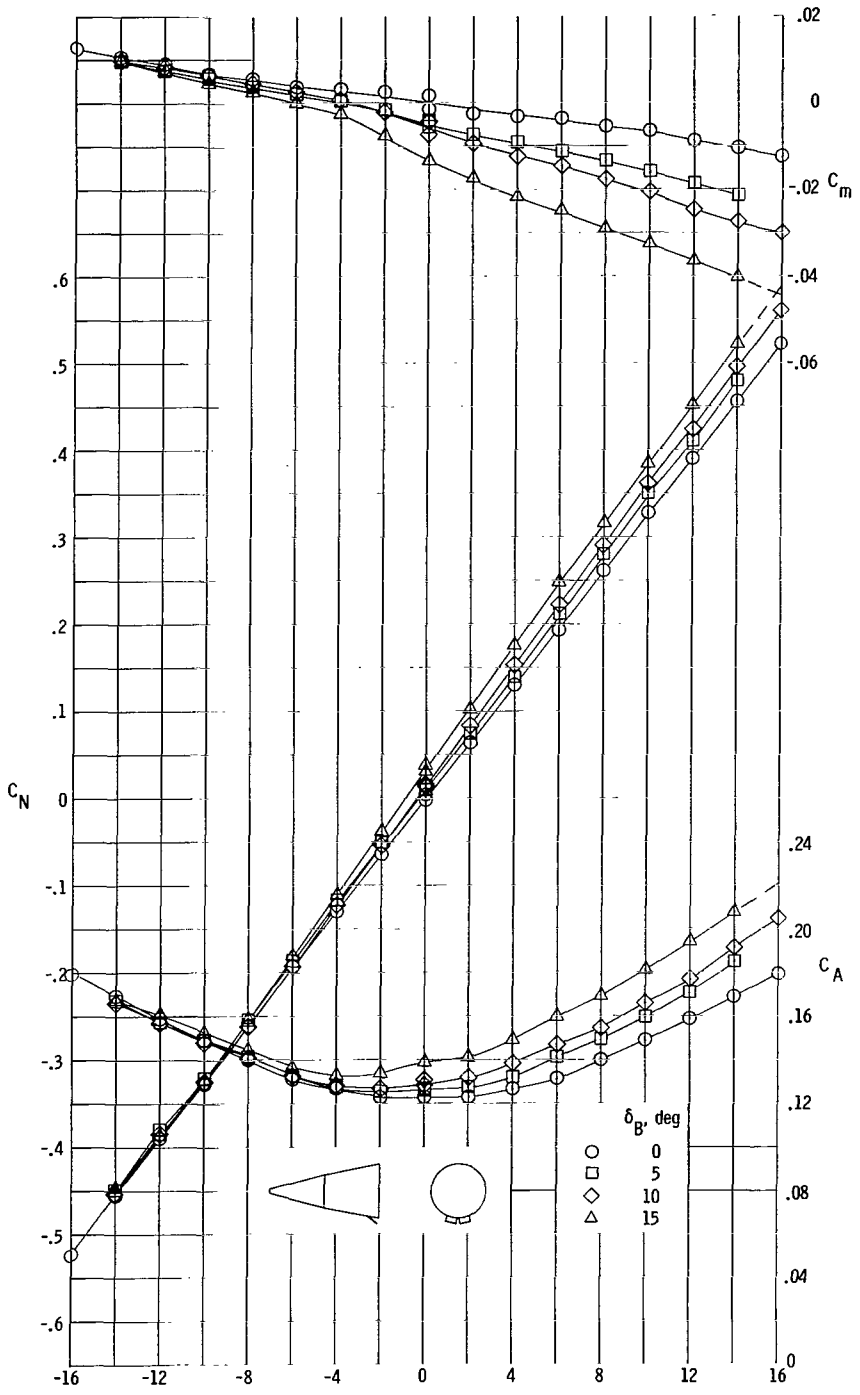

(a) Pitching-moment, normal-force, and axial-force coefficients.

Figure 5.- Basic longitudinal data for model 1 with various deflections of the two bottom flaps. M = 6.9; R = 0.98 × 10^6.

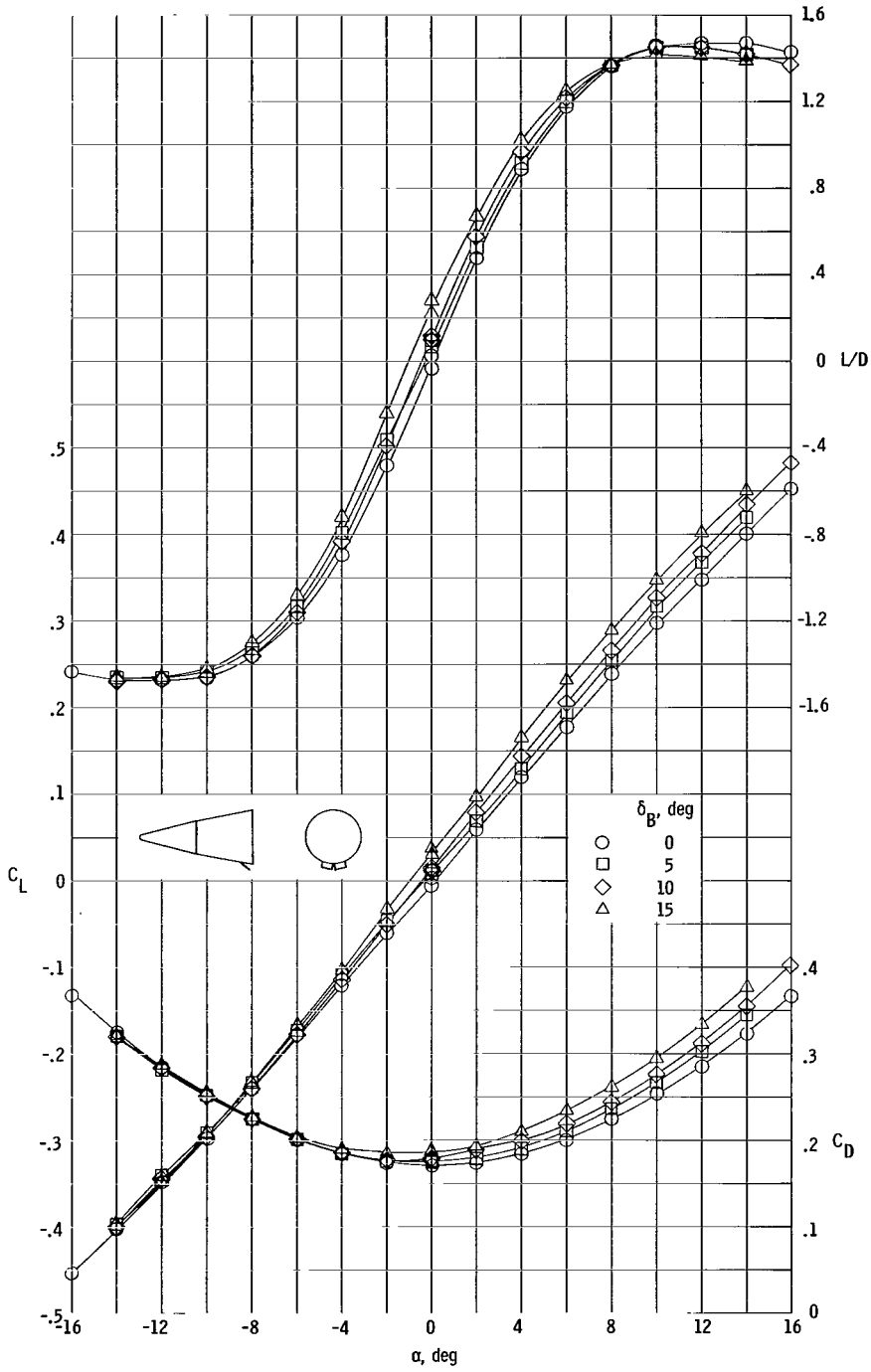

(b) Lift-drag ratio, lift coefficient, and drag coefficient.

Figure 5.- Concluded.

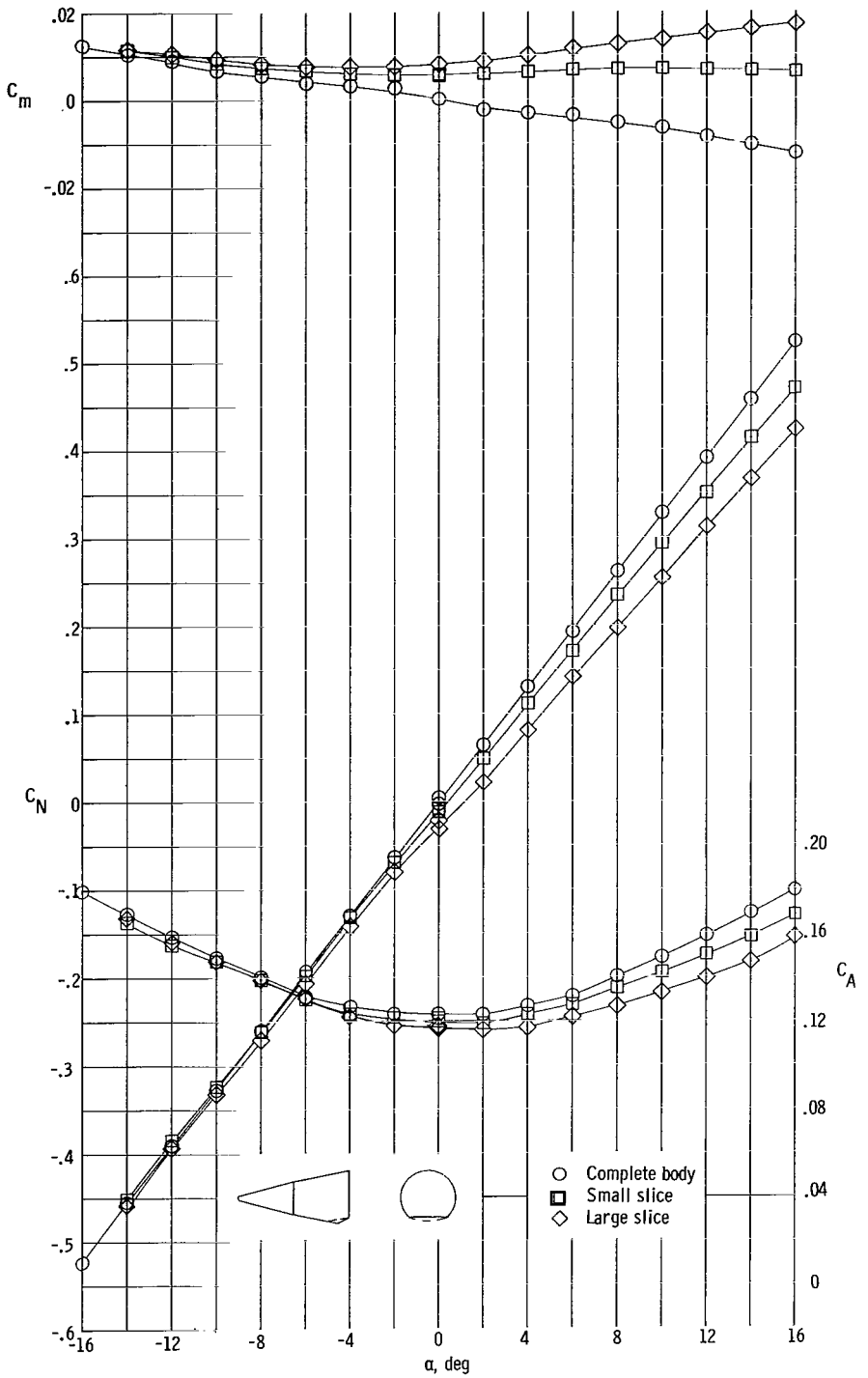

(a) Pitching-moment, normal-force, and axial-force coefficients.

Figure 6.- Basic longitudinal data for model 1a after removal of various afterbody slices. M = 6.9; R = 0.98 × 10^6; x_{cg}/l = 0.62.

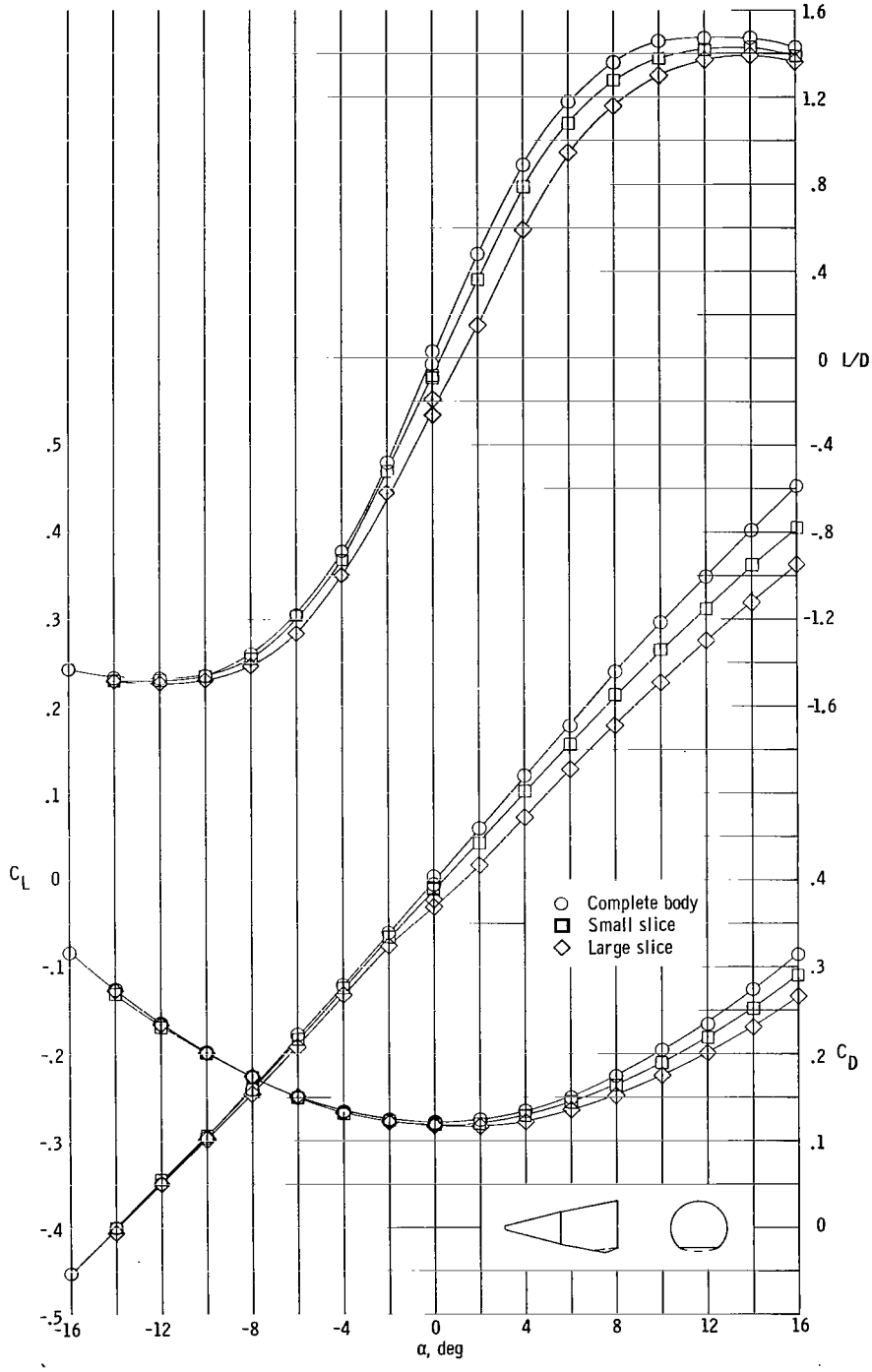

(b) Lift-drag ratio, lift coefficient, and drag coefficient.

Figure 6.- Concluded.

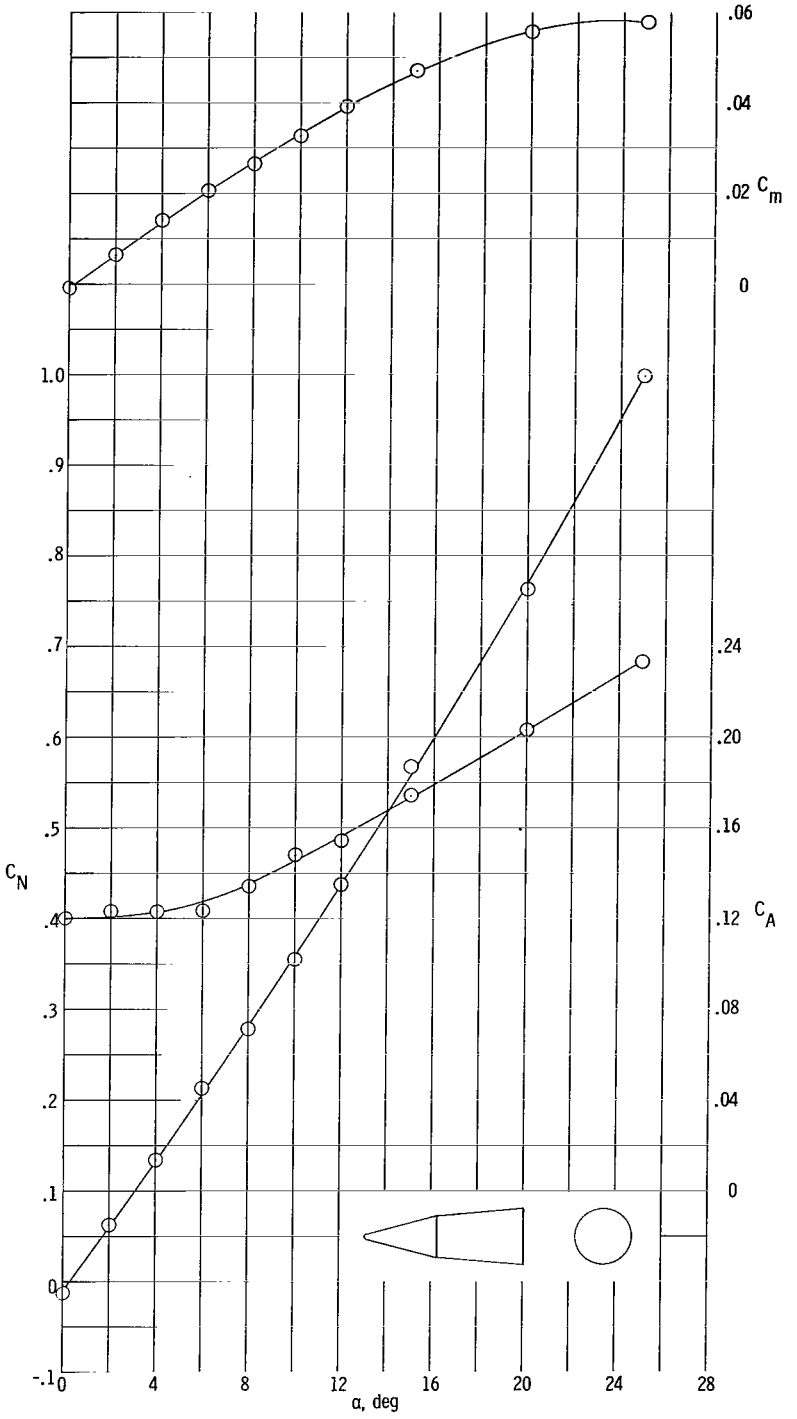

(a) Pitching-moment, normal-force, and axial-force coefficients.

Figure 7.- Basic longitudinal data for model 2. $M = 6.9$; $R = 0.98 \times 10^6$.

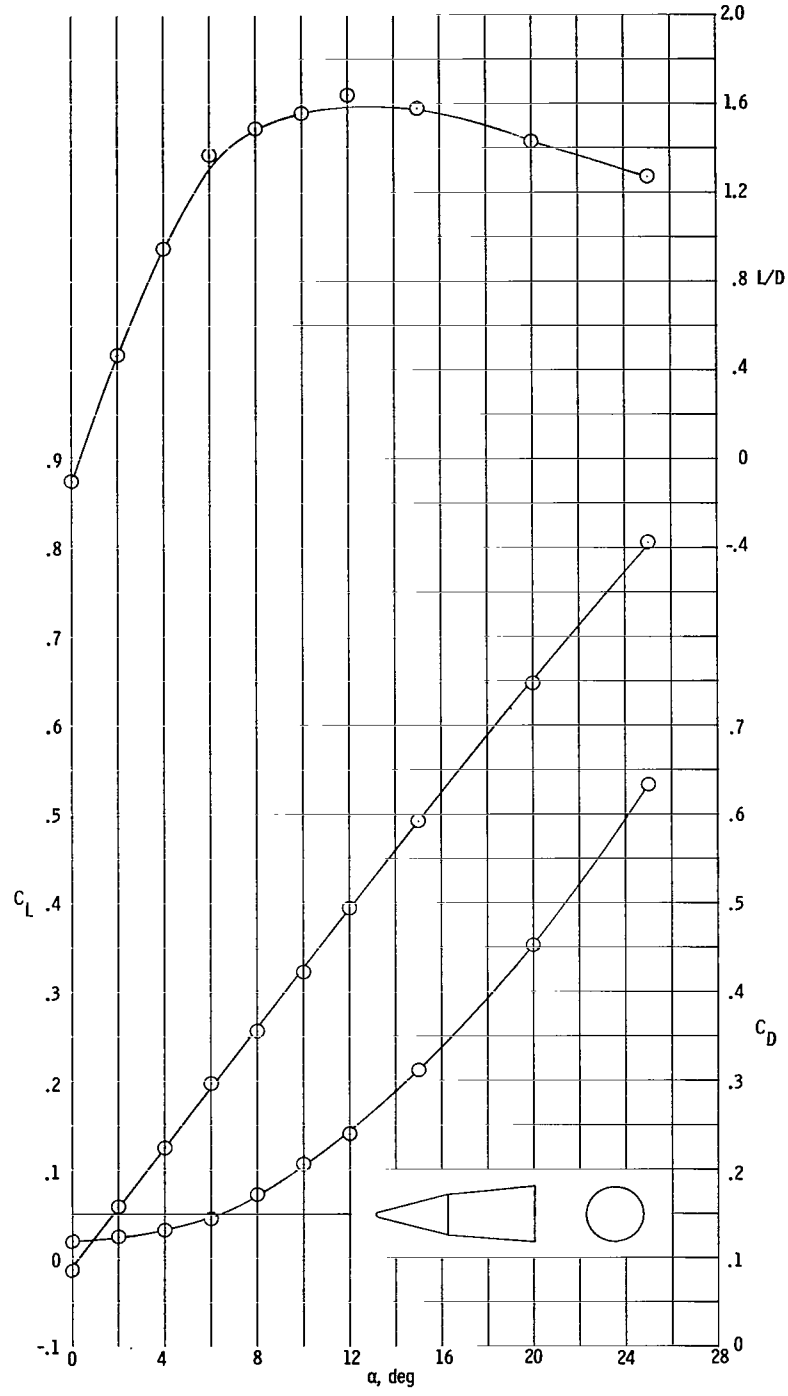

(b) Lift-drag ratio, lift coefficient, and drag coefficient.

Figure 7.- Concluded.

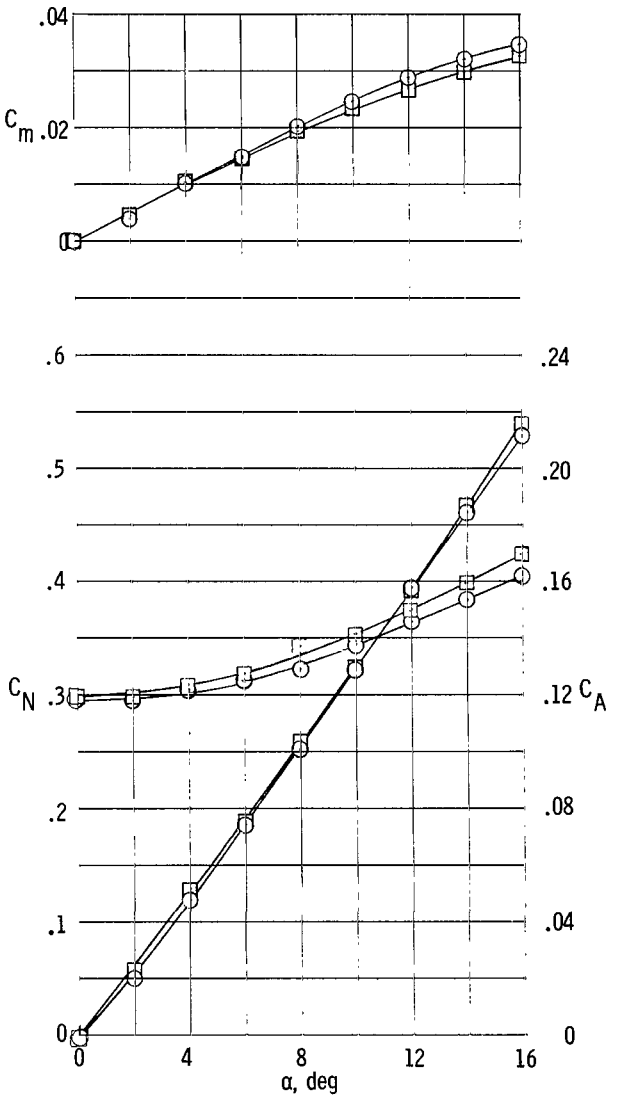

(a) Pitching moment, normal force, and axial force.

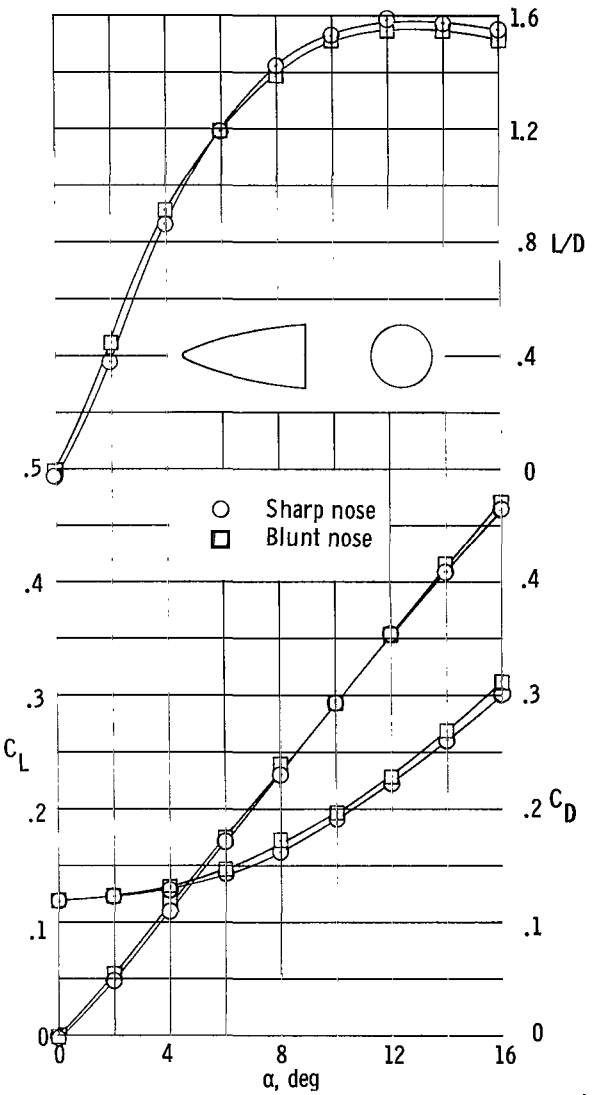

(b) Lift-drag ratio, lift, and drag.

Figure 8.- Basic longitudinal data for model 3 with both sharp and blunt nose. M = 6.9; R = 0.98×10^6.

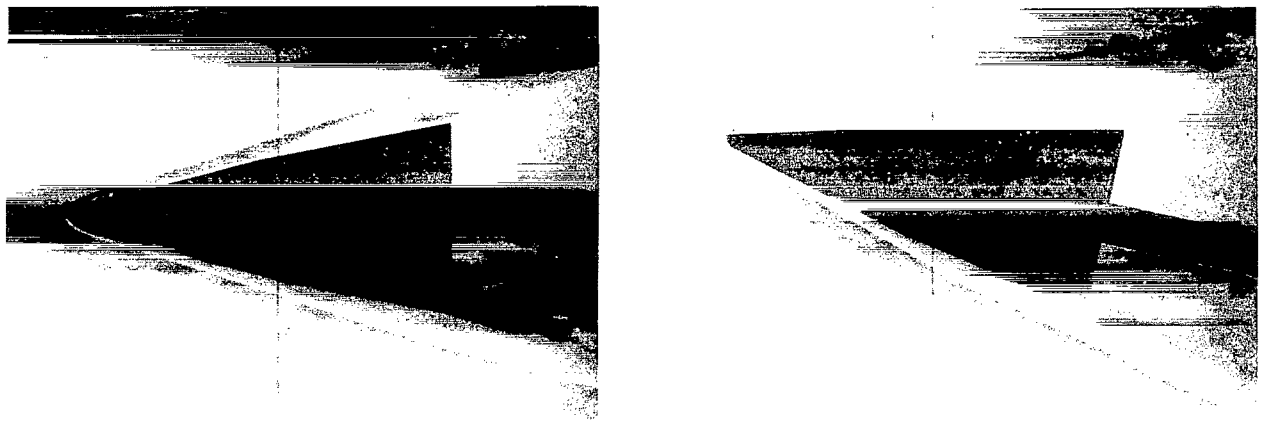

$\alpha = 0^{o}$ $\alpha = 12^{o}$

(a) Model 1; $\delta_B = 0^{o}$.

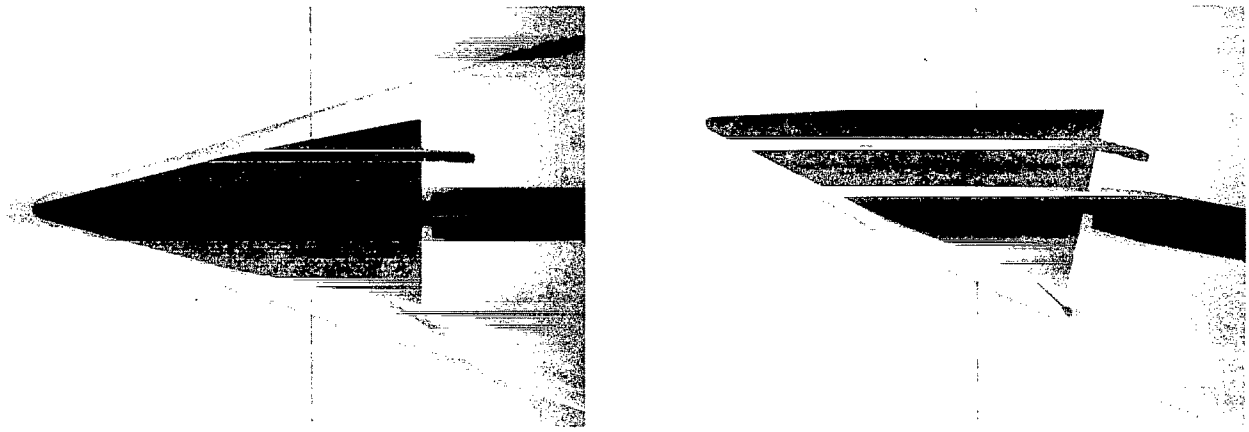

$\alpha = 0^{o}$ $\alpha = 12^{o}$

(b) Model 1; $\delta_B = 20^{o}$. L-67-960

Figure 9.- Schlieren photographs of model 1. M = 6.9; R = 0.98×10^{6}.

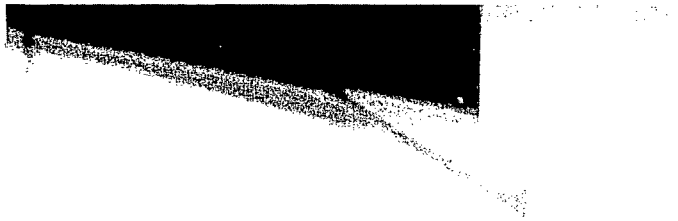

(a) Model 1; $\delta_B = 20^0$; $\alpha = 0^0$.

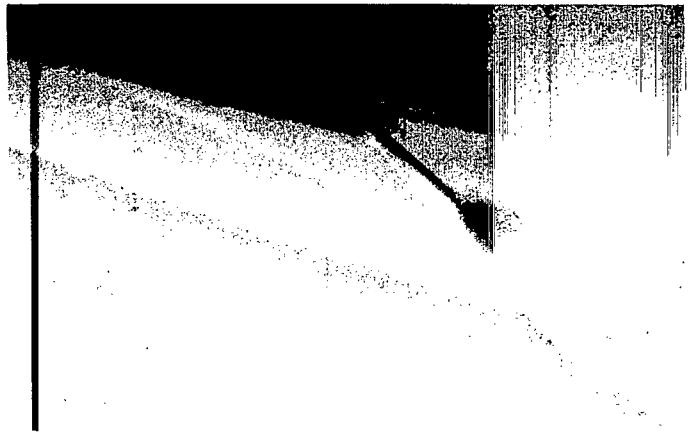

(b) Model 1; $\delta_B = 30^0$; $\alpha = 0^0$.

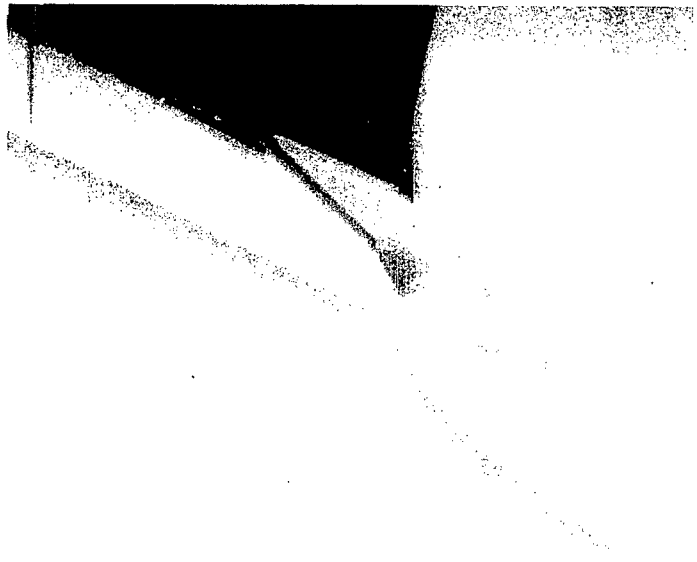

(c) Model 1; $\delta_B = 20^0$; $\alpha = 12^0$.

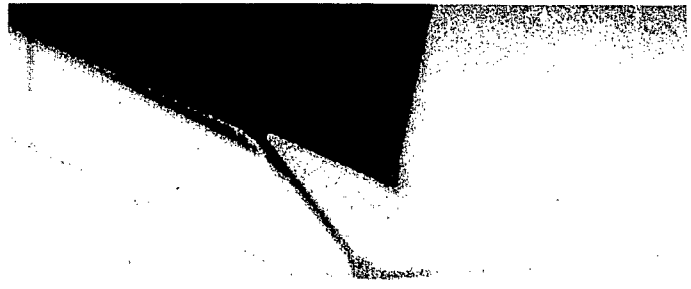

(d) Model 1; $\delta_B = 30^0$; $\alpha = 12^0$.

L-67-961

Figure 10.- Schlieren photographs of region of flaps of model 1. $M = 6.9$; $R = 0.98 \times 10^6$.

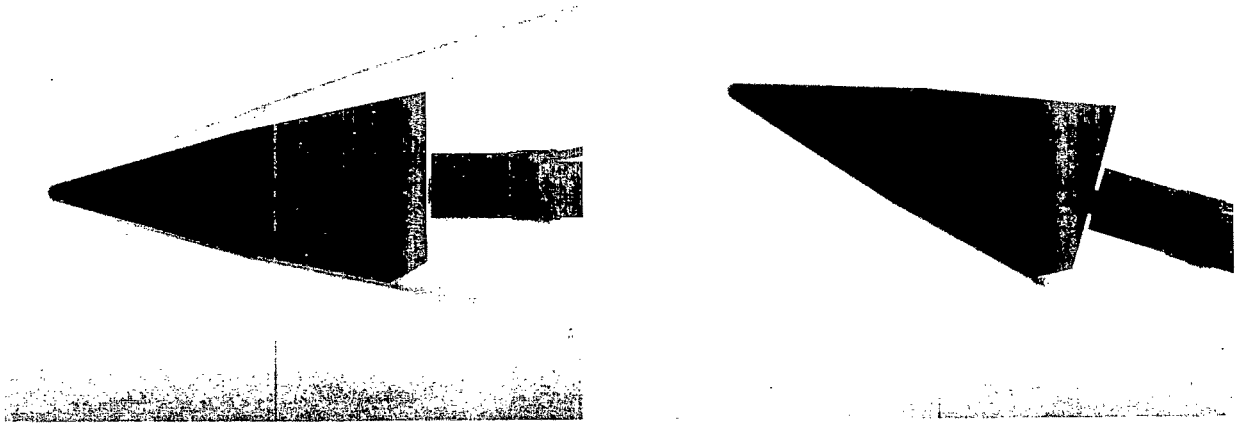

(a) Model 1a; n/d = 0.20.

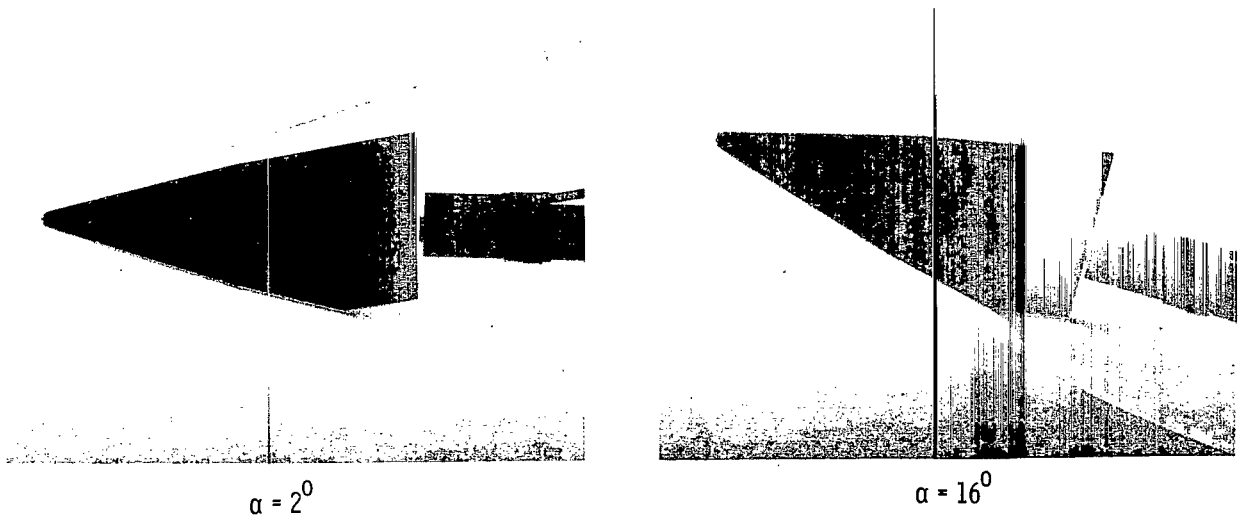

(b) Model 1a; n/d = 0.40.

L-67-962

Figure 11.- Schlieren photographs of model 1a. M = 6.9; R = 0.98 × 10^6.

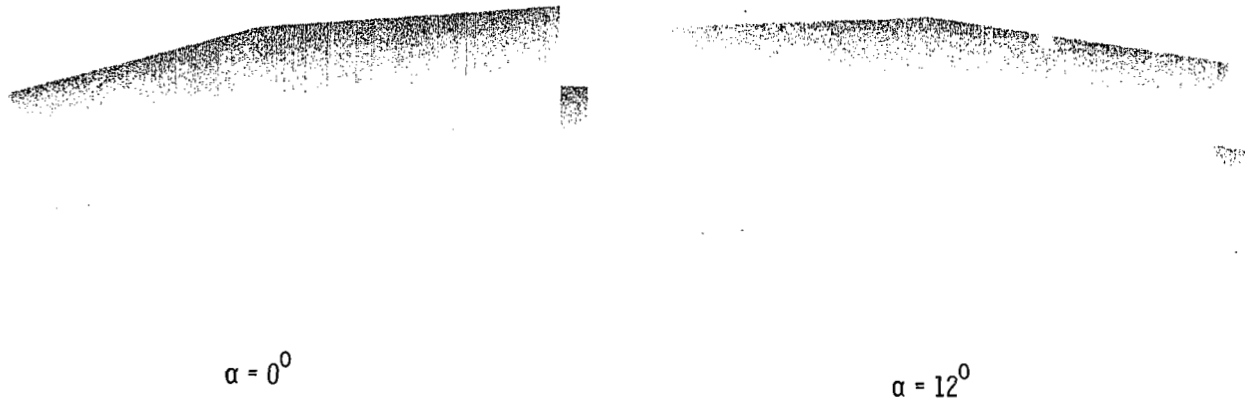

$\alpha = 0^0$ $\alpha = 12^0$

(a) Model 2.

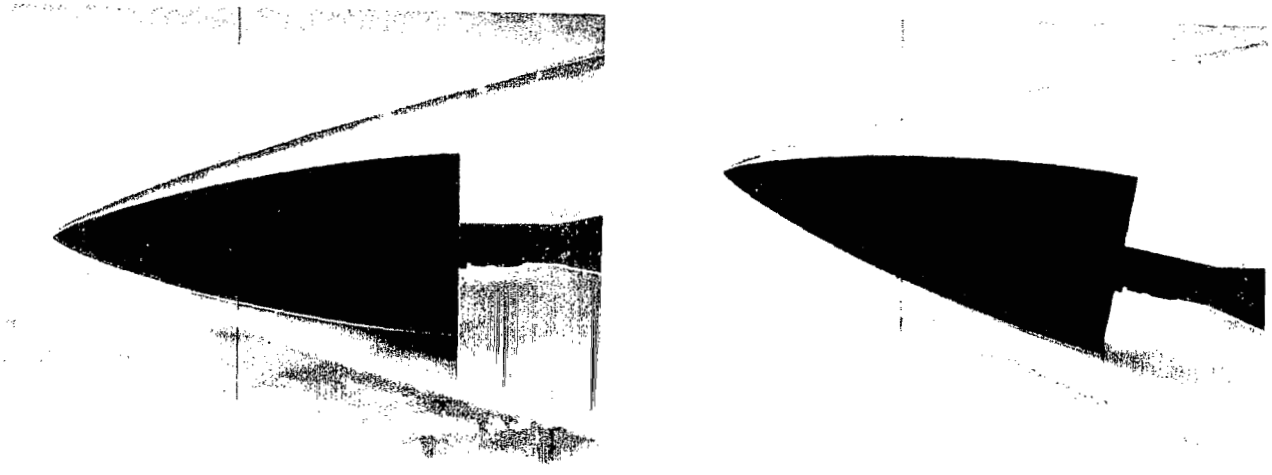

$\alpha = 0^0$ $\alpha = 12^0$

(b) Model 3.

L-67-963

Figure 12.- Schlieren photographs of models 2 and 3. $M = 6.9$; $R = 0.98 \times 10^6$.

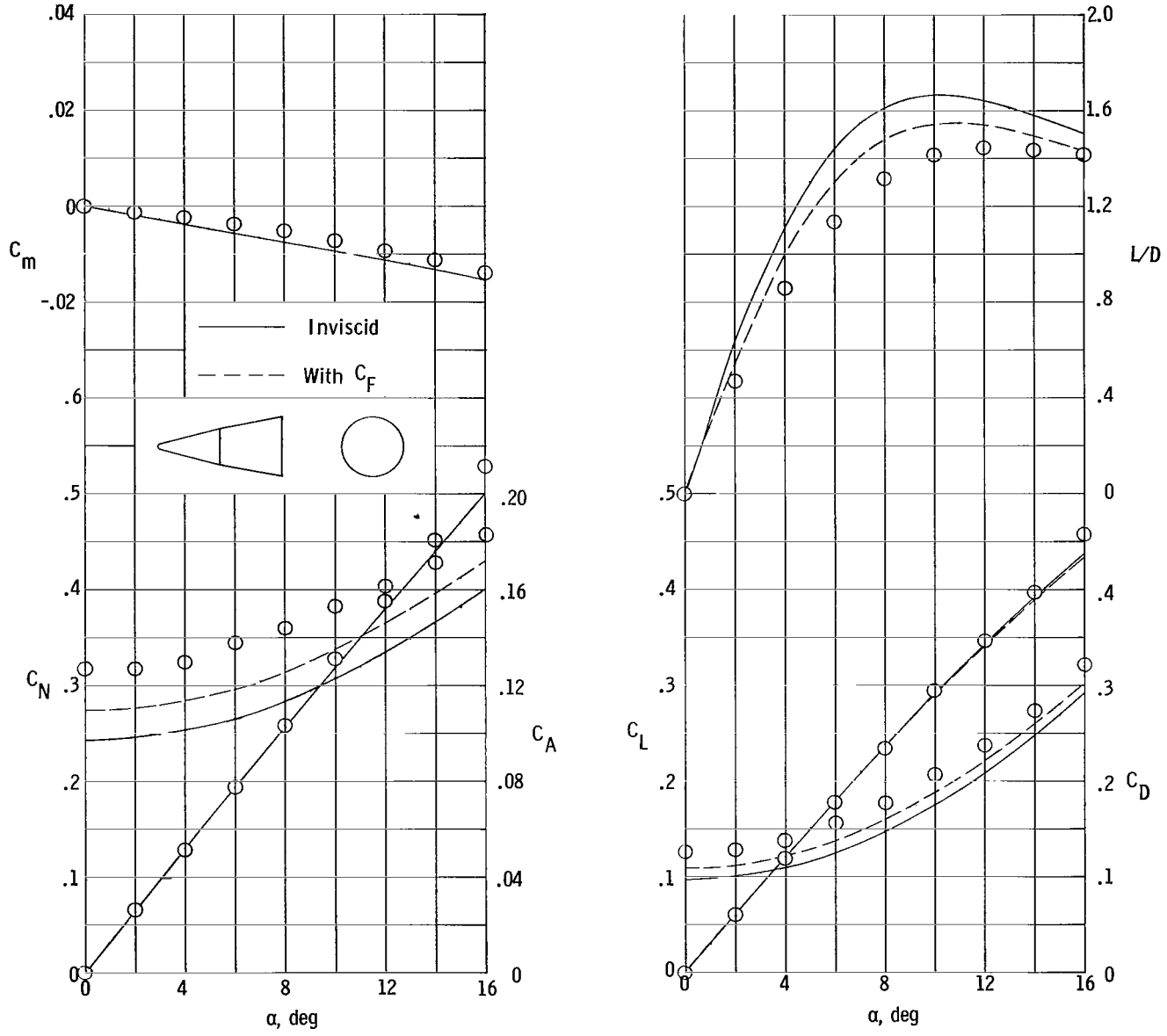

(a) Model 1.

Figure 13.- Comparison of longitudinal characteristics of models 1, 2, and 3 with Newtonian theory. M = 6.9; R = 0.98×10^6.

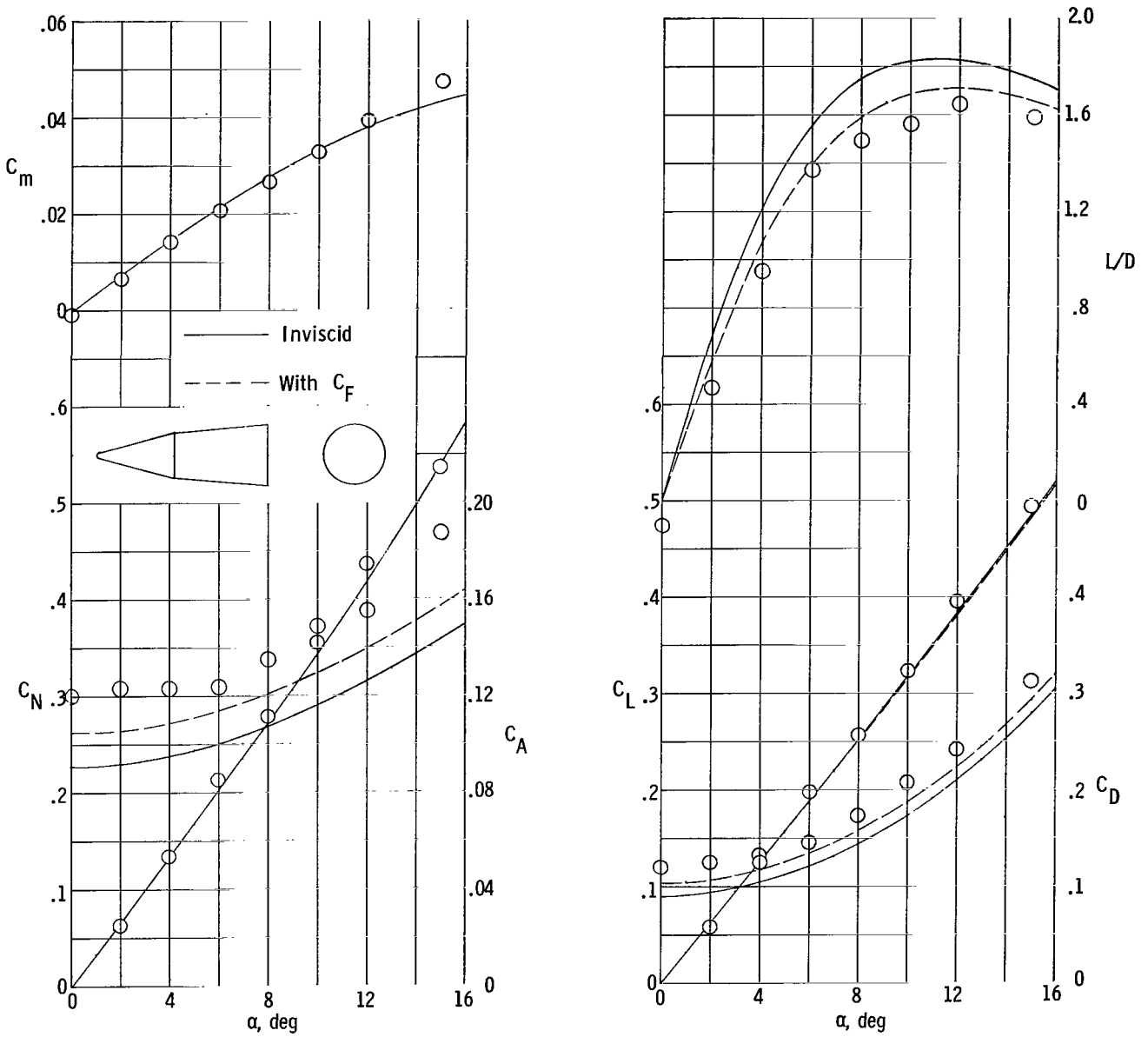

(b) Model 2.

Figure 13.- Continued.

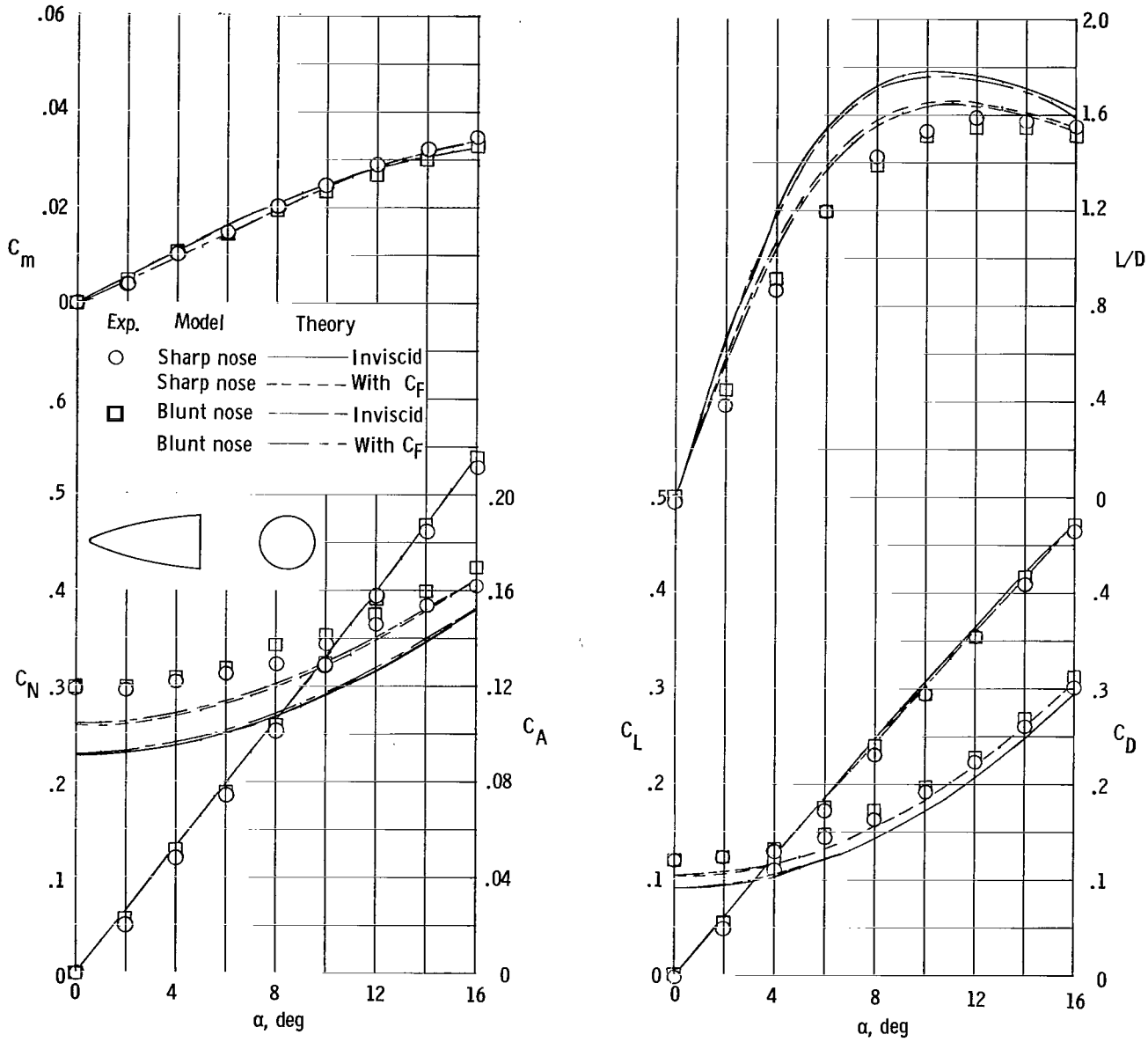

(c) Model 3.

Figure 13.- Concluded.

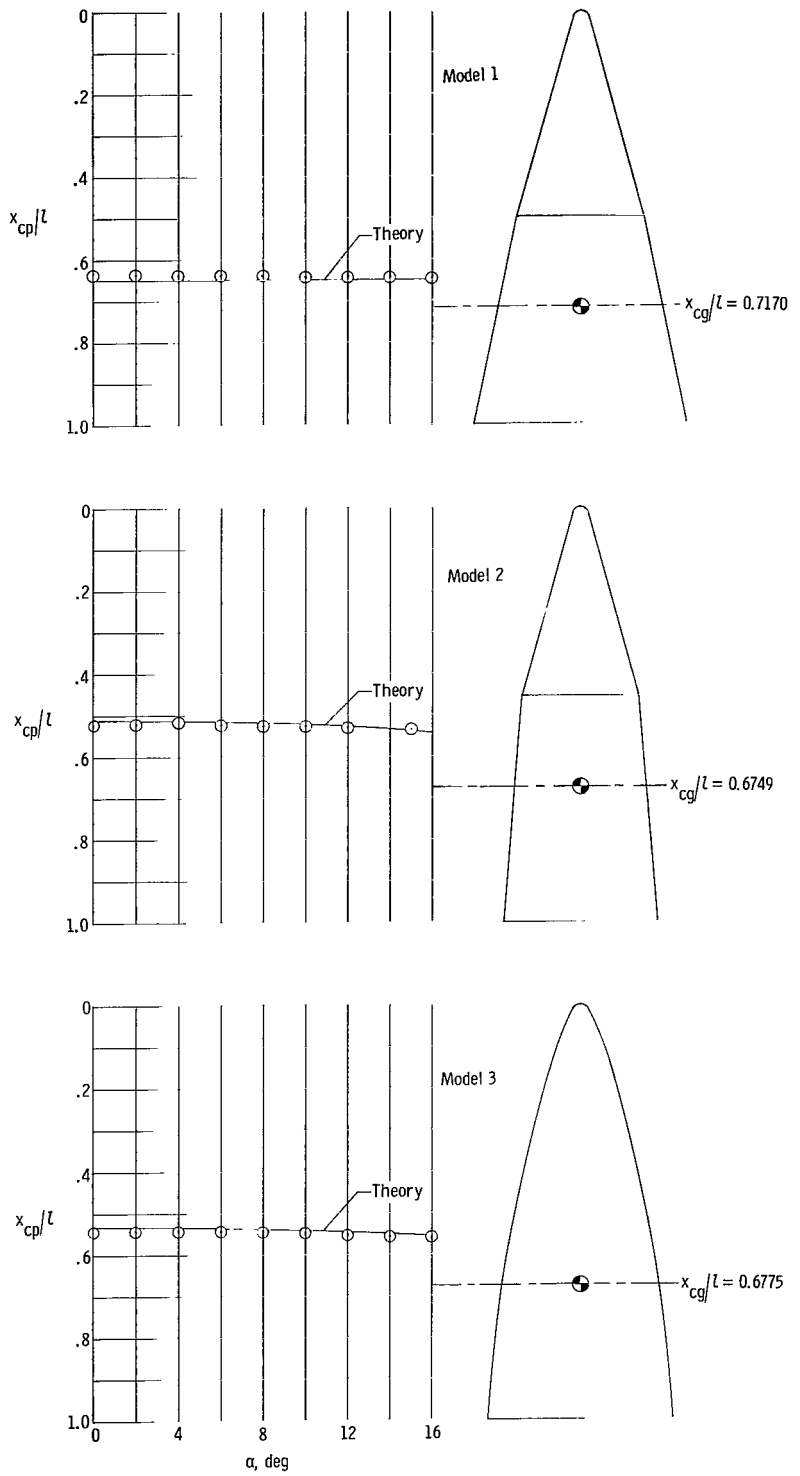

Figure 14.- Variation of center-of-pressure location with angle of attack and comparison of center-of-pressure locations with center-of-gravity locations of homogeneous bodies. M = 6.9.

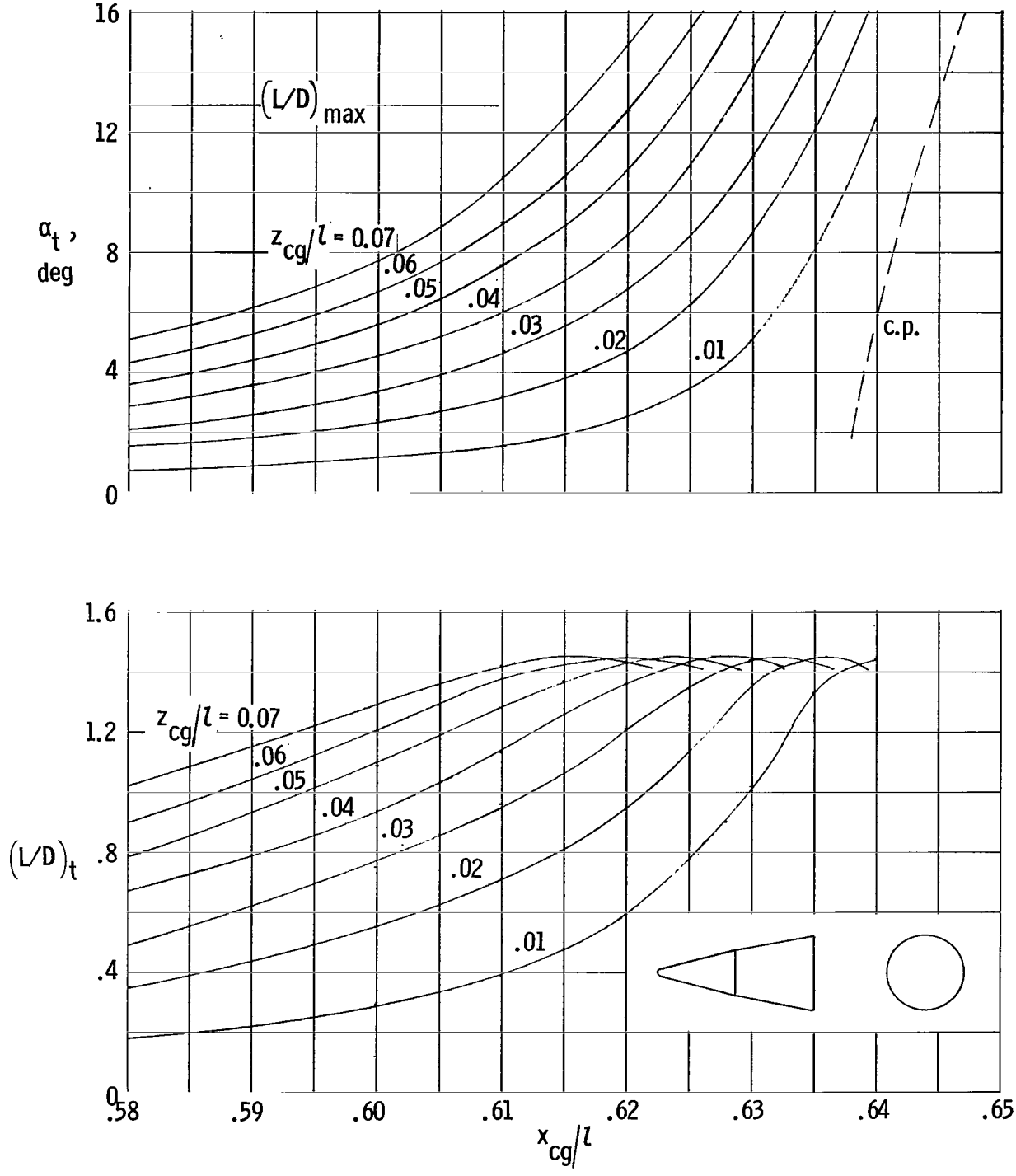

Figure 15.- Variation of trim angle of attack and trim lift-drag ratio with vertical and horizontal center-of-gravity location for model 1 without flaps. M = 6.86; R = 0.98×10^6.

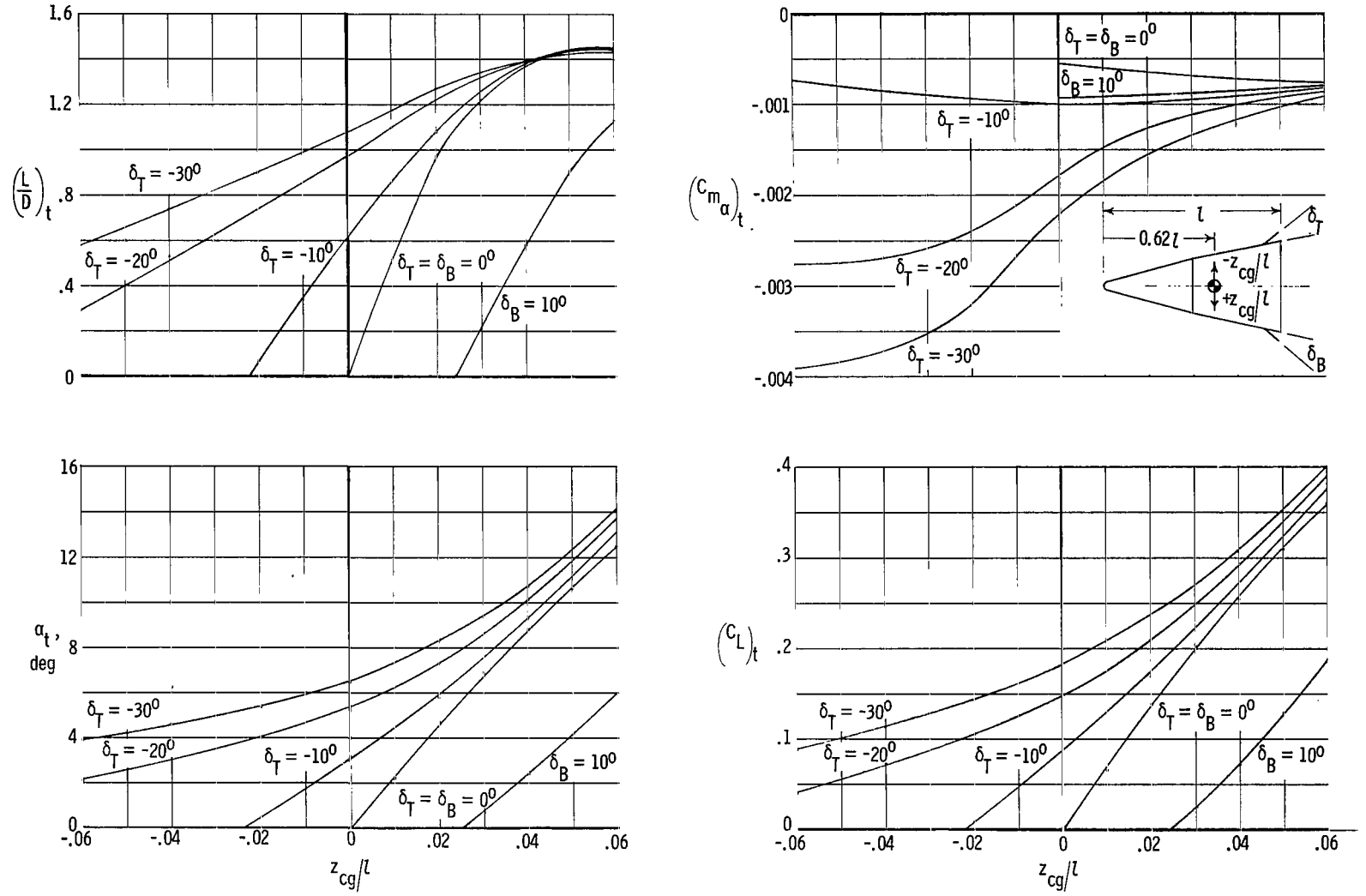

Figure 16.- Longitudinal characteristics at trim $(C_m = 0)$ of model 1 with various control deflections and vertical center-of-gravity locations. $x_{cg}/l = 0.62$; $M = 6.9$; $R = 0.98 \times 10^6$.

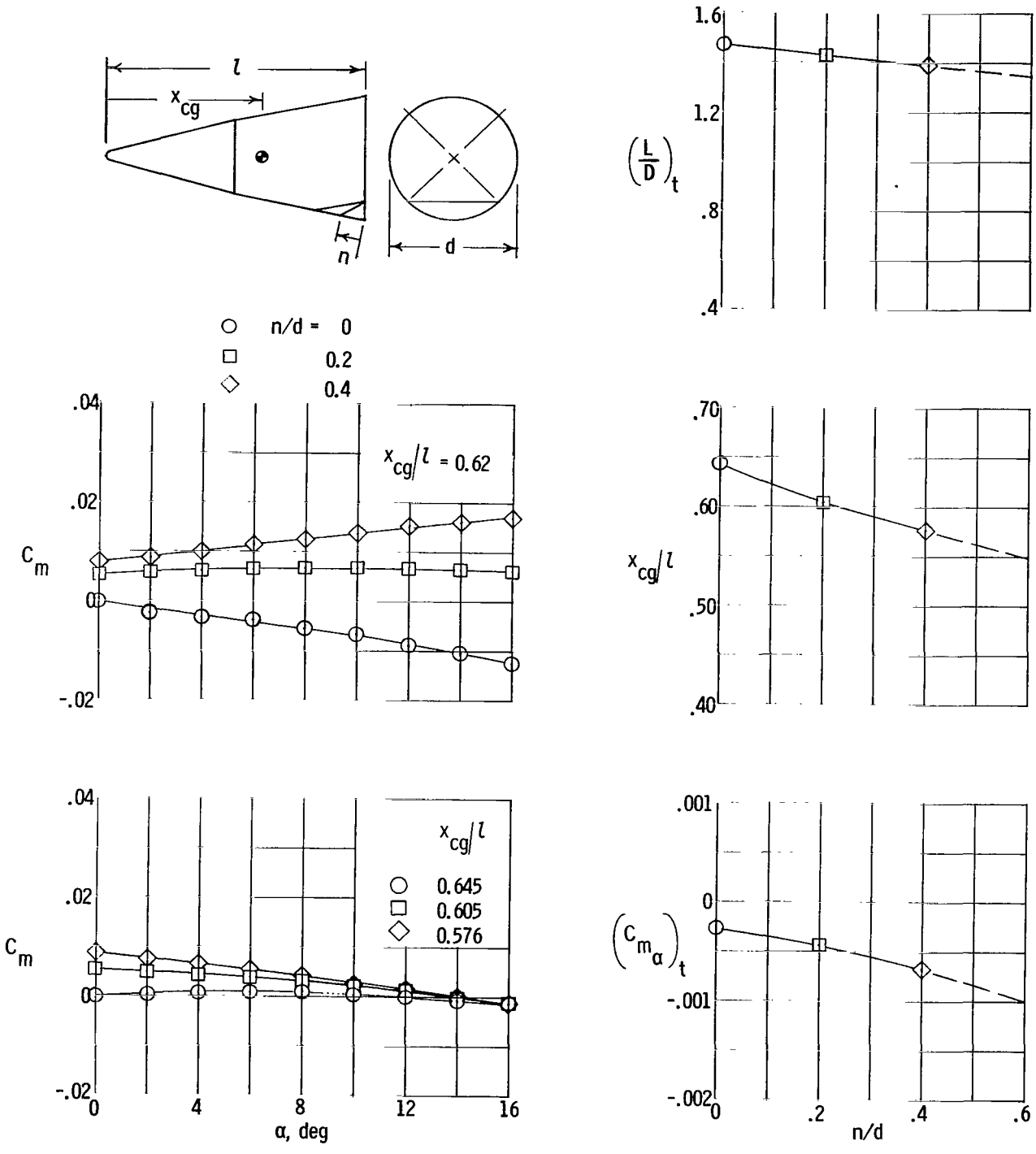

Figure 17.- A study of the use of afterbody slice for trim on model 1a. M = 6.9; R = 0.98 × 10^6.

"The aeronautical and space activities of the United States shall be conducted so as to contribute . . . to the expansion of human knowledge of phenomena in the atmosphere and space. The Administration shall provide for the widest practicable and appropriate dissemination of information concerning its activities and the results thereof."

—NATIONAL AERONAUTICS AND SPACE ACT OF 1958

NASA SCIENTIFIC AND TECHNICAL PUBLICATIONS

TECHNICAL REPORTS: Scientific and technical information considered important, complete, and a lasting contribution to existing knowledge.

TECHNICAL NOTES: Information less broad in scope but nevertheless of importance as a contribution to existing knowledge.

TECHNICAL MEMORANDUMS: Information receiving limited distribution because of preliminary data, security classification, or other reasons.

CONTRACTOR REPORTS: Scientific and technical information generated under a NASA contract or grant and considered an important contribution to existing knowledge.

TECHNICAL TRANSLATIONS: Information published in a foreign language considered to merit NASA distribution in English.

SPECIAL PUBLICATIONS: Information derived from or of value to NASA activities. Publications include conference proceedings, monographs, data compilations, handbooks, sourcebooks, and special bibliographies.

TECHNOLOGY UTILIZATION PUBLICATIONS: Information on technology used by NASA that may be of particular interest in commercial and other non-aerospace applications. Publications include Tech Briefs, Technology Utilization Reports and Notes, and Technology Surveys.

Details on the availability of these publications may be obtained from:

SCIENTIFIC AND TECHNICAL INFORMATION DIVISION

NATIONAL AERONAUTICS AND SPACE ADMINISTRATION

Washington, D.C. 20546